Advances in Colloid and Interface Science 254 (2018) 76–93

Contents lists available at ScienceDirect

Advances in Colloid and Interface Science

journal homepage: www.elsevier.com/locate/cis

Historical perspective

BiOX (X = Cl, Br, I) photocatalytic nanomaterials: Applications for fuels and environmental management

Yang Yang [1], Chen Zhang [1], Cui Lai [1], Guangming Zeng *, Danlian Huang *, Min Cheng, Jiajia Wang, Fei Chen, Chengyun Zhou, Weiping Xiong

College of Environmental Science and Engineering, Hunan University, Changsha 410082, PR China
Key Laboratory of Environmental Biology and Pollution Control, Ministry of Education, Hunan University, Changsha 410082, PR China

ARTICLE INFO

Available online 20 March 2018

Keywords:
Bismuth oxyhalides
Photocatalysis
Water splitting
CO_2 reduction
Environmental management

ABSTRACT

Energy and environmental issues are the major concerns in our contemporary "risk society". As a green technique, photocatalysis has been identified as a promising solution for above-mentioned problems. In recent decade, BiOX (X = Cl, Br, I) photocatalytic nanomaterials have sparked numerous interest as economical and efficient photocatalysts for energy conversion and environmental management. The distinctive physicochemical properties of BiOX nanomaterials, especially their energy band structures and levels as well as relaxed layered nanostructures, should be responsible for the visible-light-driven photocatalytic performance improvement, which could be utilized in dealing with the global energy and environmental challenges. In this review, recent advances for the enhancement of BiOX photocatalytic activity are detailedly summarized. Furthermore, the applications of BiOX photocatalysts in water splitting and refractory organic pollutants removal are highlighted to offer guidelines for better development in photocatalysis. Particularly, no relative reports in previous studies were documented in CO_2 reduction as well as heavy metals and air pollutants removal, thus this review presented as a considerable research value. Challenges in the construction of high-performance BiOX-based photocatalytic systems are also discussed. With the exponential growth of studies on BiOX photocatalytic nanomaterials, this review provides unique and comprehensive perspectives to design BiOX-based photocatalytic systems with superior visible light photocatalytic activity. The knowledge of both the merits and demerits of BiOX photocatalysts are updated and provided as a reference.

Contents

* Corresponding authors at: College of Environmental Science and Engineering, Hunan University, Changsha 410082, PR China.
E-mail addresses: zgming@hnu.edu.cn (G. Zeng), huangdanlian@hnu.edu.cn (D. Huang).
[1] These authors contribute equally to this article.

https://doi.org/10.1016/j.cis.2018.03.004
0001-8686/

1. Introduction

With the rapid industrialization and urbanization, energy shortages and environmental pollutions have aroused considerable concerns from the world [1–4]. Semiconductor photocatalysis, as one of the most prospective ways to tackle these problems, including hydrogen (H_2) and oxygen (O_2) production from water [5,6], carbon dioxide (CO_2) reduction to energy-bearing carbon fuels [7,8] and organic pollutants decomposition [9,10], has become the focus of study because it is a "green" technology in facing clean energy demand and tackling environmental issues [11].

As far back as 1972, Fujishima and Honda first discovered that water can be split into H_2 and O_2 by irradiating a TiO_2 anode connected with a Pt black cathode via an external bias, indicating water can be directly decomposed into H_2 and O_2 under visible light irradiation with the assistance of catalysts [12]. From then on, great efforts have been made in semiconductor photocatalysis [13–17]. Among the traditional photocatalysts, TiO_2 has been extensively used as an effective photocatalyst for water splitting and complete organic contaminants degradation under ultraviolet (UV) light irradiation. However, it can only induce photons in UV light region which approximately accounts for ~4% of the solar light because of its high band gap energy (3.0–3.2 eV) [8,10,18].

As for solar light, visible light is easily obtained across the earth, which accounts for about 50%. Thus, considerable attention has been drawn to the research of visible-light-active photocatalysts [19,20]. And it has been found that the orbitals of certain p-block metals can hybridize O 2p orbitals to form a better hybridized valence band (VB), such as Ag 4d orbitals in Ag(I), Bi 6 s orbitals in Bi(III) and Sn 5 s orbitals in Sn(II), enhancing the mobility of photo-generated charge carriers, narrowing their band gaps and promoting the absorption of visible light [6,21]. Considering of the advantages such as earth abundance, stability, economic and toxicity, bismuth-based (Bi-based) materials are more sustainable photocatalysts; besides, most Bi-based semiconductors have shown efficient photocatalytic activities towards water splitting, CO_2 reduction and harmful pollutants removal under visible light irradiation [22,23]. On the basis of the above merits, our team have successfully developed some excellent Bi-based visible-light-active photocatalysts, such as Ag/g-C_3N_4/$BiVO_4$ [14], g-C_3N_4/Bi_2WO_6 [24], Bi/BiOCl/ZnSn(OH)$_6$ [25] and Ag_3PO_4/Ag/$BiVO_4$ [26]. As shown in Fig. 1a, an exponential growth of relative publications was reported on Bi-based photocatalysts for energy conversion and environmental management (according to ISI Web of Science™ from 2006 to 2016).

Meanwhile, similar increasing trend in interest is also detected with regards to bismuth oxyhalides (BiOX (X = Cl, Br, I)) photocatalysts (Fig. 1b–d). BiOX (X = Cl, Br, I), as one kind of important Bi-based

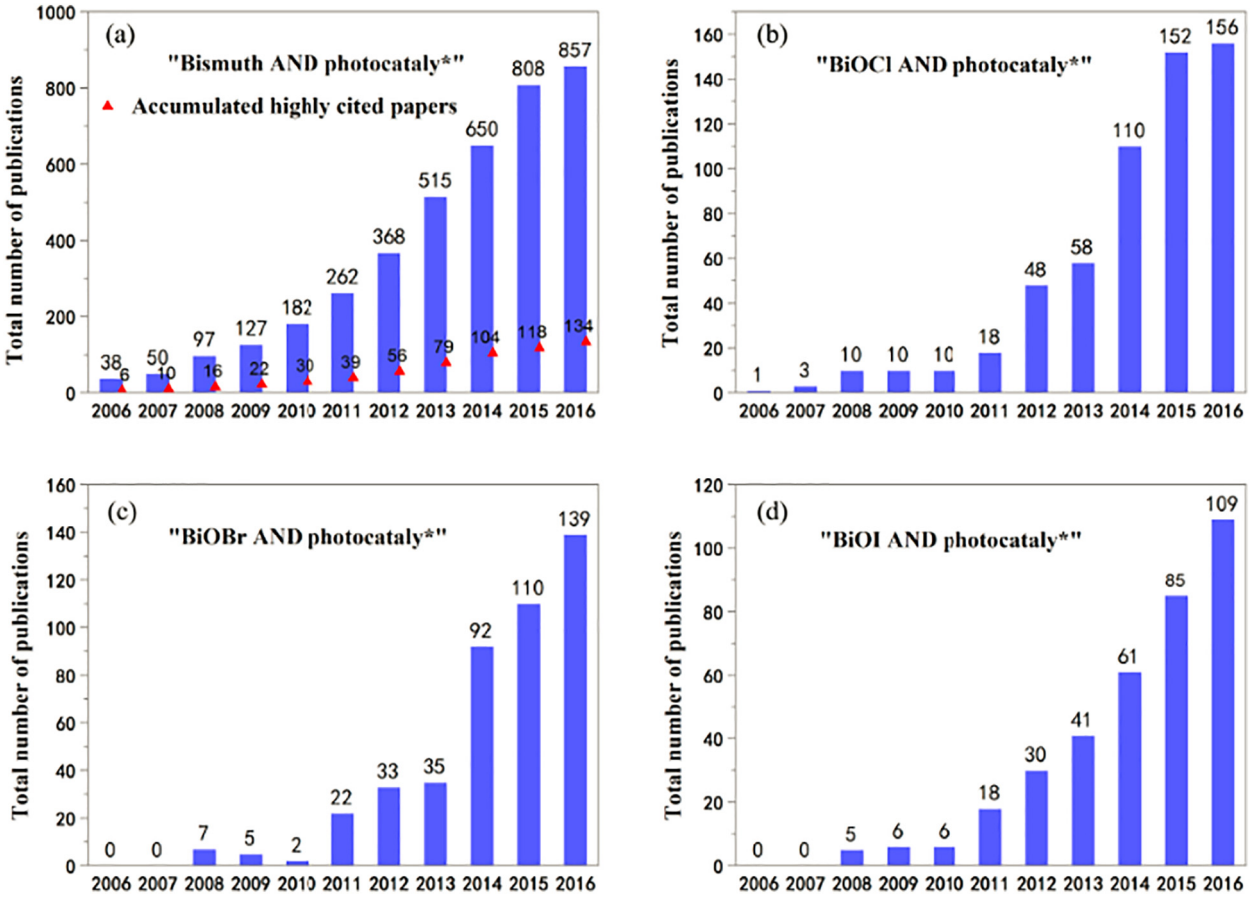

Fig. 1. Increasing interest in bismuth-based photocatalysts and bismuth oxyhalides. The charts display the total number of publications per year about (a) bismuth-based photocatalysis, (b) BiOCl photocatalysis, (c) BiOBr photocatalysis and (d) BiOI photocatalysis.

photocatalysts, should benefit from their complex band structures and unique layered structures. The band structures of these BiOX are illustrated in Fig. 2 [27], the top of the VB and the bottom of the conduction band (CB) are located in the R and Z point, respectively, suggesting they are indirect band gap semiconductors. That is to say the photo-induced electrons on BiOX should pass a certain k-space distance from the VB to arrive in the CB, further to reduce the photo-induced electrons and holes recombination rate [27–29]. All BiOX semiconductors possess a tetragonal matlockite structure, as shown in Fig. 3, BiOX displayed relaxed layered structures with $[Bi_2O_2]$ slabs inserting into double halogen atom slabs [30]. The layered structure of BiOX can offer enough space to polarize the related atoms and orbitals, which can excite the formation of an internal electric field (IEF) between $[Bi_2O_2]$ and halogen slabs. And because the induced IEF can accelerate the separation and migration of photo-excited electron-hole pairs, the photocatalytic activities of BiOX are improved significantly [27–29,31]. Throughout the above analyses, it is reasonable to carry out more investigations on BiOX photocatalysis.

Several reviews about BiOX photocatalytic nanomaterials have been published, but most of them focus on BiOX nanostructures and organic pollutants degradation [30,32,33]. Nevertheless, the applications of this series of photocatalysts in the fields of fuel production and removal of heavy metals and air pollutants have not been reviewed, which are indispensable fields of the present study. In this review, we sum up the recent strategies for the enhancement of BiOX photocatalytic activity under visible light and their applications in water splitting and degradation of organic pollutants, especially in the fields of CO_2 reduction as well as removal of heavy metals and air contaminants. This review is finished by the discussion on crucial challenges that exist in the use of BiOX nanomaterials to resolve energy and environmental issues, and giving suggestions and new directions in constructing BiOX-based photocatalytic systems with high performance.

2. Properties of BiOX nanomaterials

Chlorine (Cl), bromine (Br), and iodine (I) elements are on the same main group, therefore, BiOCl, BiOBr, and BiOI might possess the similar properties. Zhang et al. [28] first revealed that the Cl 3p states and Bi 6p states respectively constitute the VB and the CB. Furthermore, Zhao et al. [27] proved that both O 2p and X np (n = 3, 4 and 5 for X = Cl, Br and I, respectively) states contribute most to the valence band maximum (VBM) while the Bi 6p states dominate the conduction band minimum (CBM). The band gaps of experimental determination for BiOCl, BiOBr, and BiOI are 3.22, 2.64, and 1.77 eV, respectively [34]. Comparatively, their theoretically calculated indirect band gaps are 2.50, 2.10 and 1.59 eV, respectively [27]. The band gaps differences between the experimental and calculated results due to the density-functional theory limitation [35]. Nevertheless, the band gaps decrease with the increase of atomic number of Cl, Br, and I elements, and their response wavelengths gradually move towards the visible light region from UV light region.

Many studies have been done to investigate the photocatalytic performance of BiOCl nanomaterials under UV light irradiation [28,36]. Zhang et al. [28] first introduced the layered BiOCl nanoplates using a hydrolysis approach. And the layered BiOCl nanoplates exhibited much better stability and UV photocatalytic activity towards methyl orange (MO) degradation than TiO_2. Moreover, Jin and co-workers [36] reported that ultrathin BiOCl nanosheets displayed high photocatalytic activity for the photoreduction of CO_2 into CH_4. Besides the surface-to-volume ratio, single-crystalline characteristics and exposed {001} facets, numerous oxygen vacancies of BiOCl nanosheets generated under UV light also contribute to the excellent photocatalytic activity towards CO_2 reduction by promoting the adsorption of CO_2 and molecular O_2. However, unmodified BiOCl only express photocatalytic activity under UV light as a result of its wide band gaps, blocking its more extensive applications.

BiOBr photocatalyst was also widely employed in recent years owing to its relatively narrow bandgap and preferable visible light photocatalytic activity [37,38]. For example, Zhang et al. [37] successfully prepared 3D flower-like BiOBr microspheres by ethylene glycol (EG) assisting solvothermal method. And high visible light photocatalytic activity was observed towards MO degradation because of its intrinsic properties such as narrow band gaps. In addition, Wu et al. [38] utilized {001} facet dominated BiOBr nanosheets to reduce CO_2 under simulated sunlight irradiation. The BiOBr nanosheets exhibited the highest CO production rate of 4.45 μmol h^{-1} g^{-1}, which was mainly ascribed to the large active surface area, effective charge carrier separation and

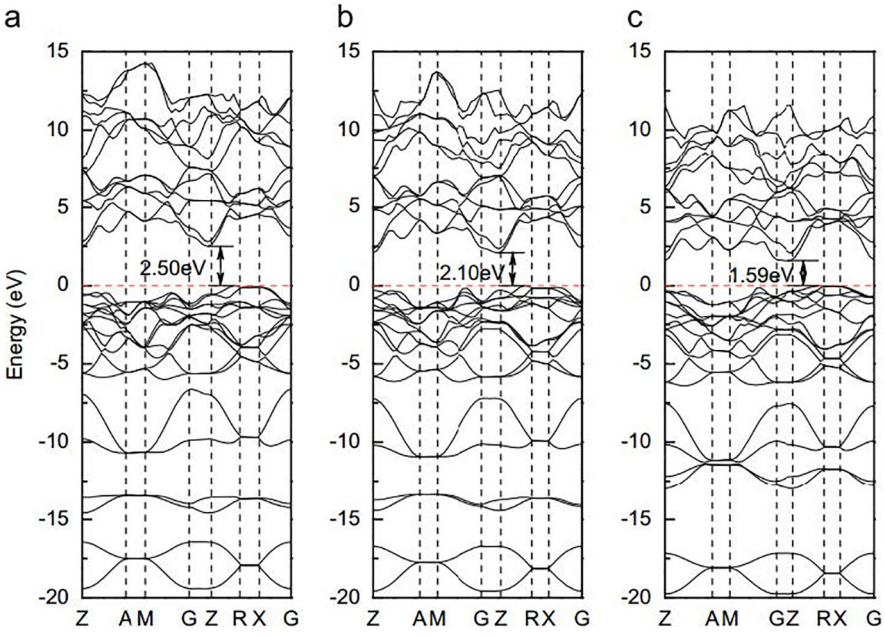

Fig. 2. Band structures of BiOX: (a) BiOCl crystals, (b) BiOBr crystals and (c) BiOI crystals. (Reprinted with permission from ref. [27]. Copyright (2012) Elsevier.)

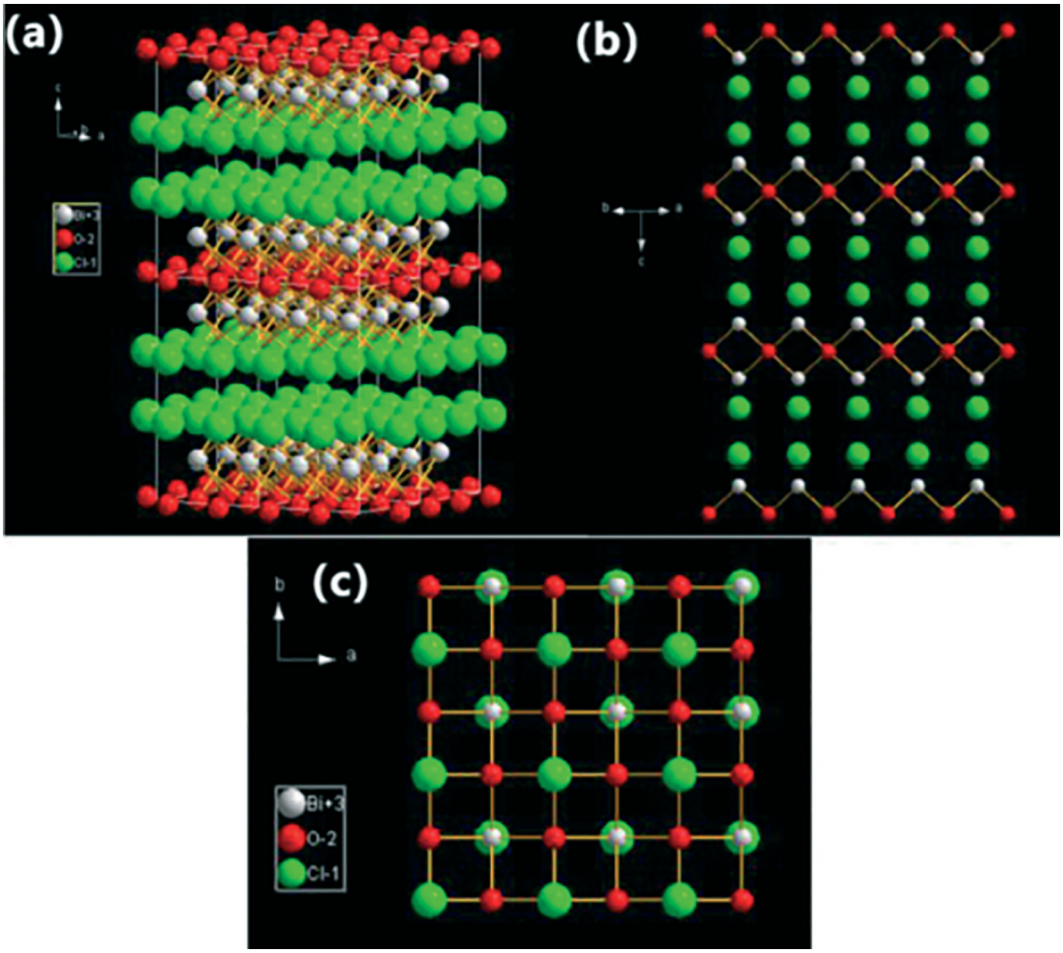

Fig. 3. Layered structure models of BiOCl: (a) three-dimensional spatial structure, (b) {110} crystal facets and (c) {001} crystal facets. (Reprinted with permission from ref. [30]. Copyright (2014) The Royal Society of Chemistry.)

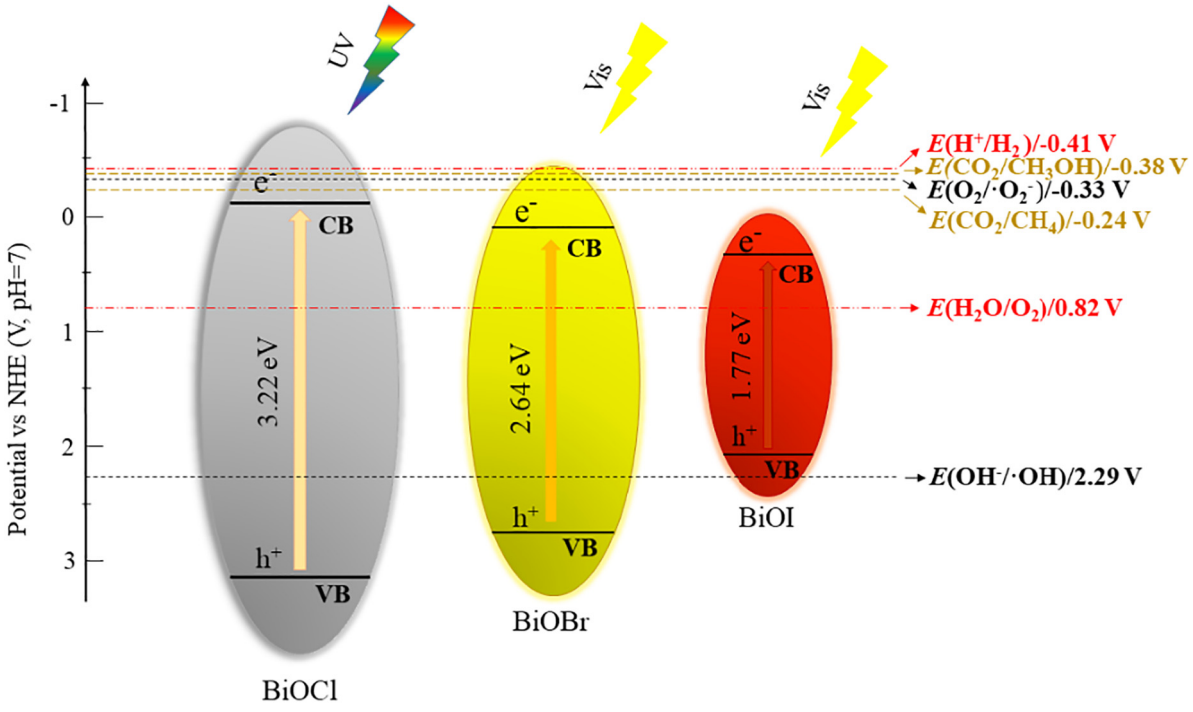

Fig. 4. Band positions of BiOX and redox potentials of different species in photocatalysis.

enhanced reduction ability. These results imply that BiOBr has favorable visible-light-driven (VLD) photocatalytic performance, especially after some modification.

As for BiOI (the narrowest bandgap in three samples), pure BiOI exhibits poor photocatalytic activity due to the inherent rapid electron-hole recombination. An et al. [39] found that BiOI could only degrade rhodamine B (RhB) to *N*-de-ethylated rhodamine under visible light. In contrast, Long et al. [40] synthesized a novel porous hierarchical BiOI nanostructures at room temperature. And the removal efficiency of RhB was about 98.7% under visible light irradiation by using this novel nanomaterial. This result shows that the morphology and structure can significantly affect the photocatalytic performance of BiOI.

BiOX nanomaterials display excellent photocatalytic potential for energy conversion and environmental management. But their relatively positive CB position and weak reduction power can't meet the demand of energy conversion and their photocatalytic efficiency is still unsatisfied under solar light irradiation, which restrict their practical applications (Fig. 4). In order to strengthen the photocatalytic performance of BiOX nanomaterials under solar light irradiation, many strategies have been used to tune the energy band position, boost the sunlight harvesting and promote the separation and transportation of photo-induced electron-hole pairs, which contains microstructure modulation, facet and defect control, carbonaceous materials compounding, heterojunction construction and so on.

3. Strategies for the enhancement of BiOX photocatalytic activity

3.1. Microstructure modulation

The physical and chemical properties of materials are extremely related to their microstructure, such as size, shape, specific surface area and dimensionality [41,42]. Among BiOX nanomaterials, there are one dimensional (1D) nanofibers [43], two dimensional (2D) nanosheets/nanoplates [44–47] and three dimensional (3D) microspheres/hierarchical nanostructures [37,48–51]. The 3D assemblies have sparked more interests owing to their distinctive architecture and excellent photocatalytic activity. Zhang et al. [48] successfully synthesized BiOI photocatalyst with flower-like hierarchical structure via direct hydrolysis method at room temperature and first utilized it for photocatalytic reduction of CO_2 to CH_4 under simulated sunlight irradiation. In detail, the total yield of CH_4 over BiOI with flower-like hierarchical structure was 0.198 μmol h^{-1} g^{-1}, while the total yield of CH_4 over bulk BiOI and TiO_2 only were 0.085 μmol h^{-1} g^{-1} and 0.015 μmol h^{-1} g^{-1}, respectively. This work shows that 3D nanostructure can efficiently enhance the photocatalytic ability of BiOI for CO_2 conversion.

Moreover, Zhao et al. [49] synthesized hierarchical BiOBr microspheres which were almost composed of sphere-like hierarchical structures with the diameter of 2–4 μm through a solvothermal method with the help of sodium dodecyl sulfate (SDS). Meanwhile, 3D flower-like BiOBr photocatalysts which were nearly made up of flower-like structures with the diameter from 3 μm to 5 μm was synthesized without SDS. Fig. 5 shows the scanning electron microscope (SEM) images of the flower-like BiOBr and sphere-like BiOBr, respectively. Although both of the samples are 3D nanostructure, the photocatalytic degradation efficiency of RhB on sphere-like BiOBr reached about 100% on 30 min under visible light. It was only 85% for flower-like BiOBr under identical conditions. This is mainly because the sphere-like BiOBr nanomaterials possess thinner self-assembled nanosheets, smaller nanocrystals and more oxygen vacancies than the flower-like BiOBr, which can provide more active sites and promote the direct photoexcitation and indirect dye photosensitization.

Hydro/solvothermal treatment is a primary method to construct 3D-structured BiOX because of its high reaction efficiency and simple experimental process [37,49–51]. The formation mechanism of 3D BiOX assemblies achieved by the hydro/solvothermal reactions usually includes the following three main steps: (i) the formation of BiOX nuclei at the forepart (ii) the growth of 2D nanosheets through a dissolution-renucleation process, and (iii) the figuration of 3D BiOX structures from the oriented aggregation of 2D nanoplates under the electrostatic multipole field [50,51]. Overall, the improved photocatalytic activity of 3D nanostructure is attributable to their enhanced light harvesting ability, curtate diffusion pathways, faster separation of photo-excited electron-hole pairs and more reactive spots.

3.2. Facet and defect control

As a basic feature of crystalline materials, the exposed crystal facets play an important role in the photocatalytic efficiency since

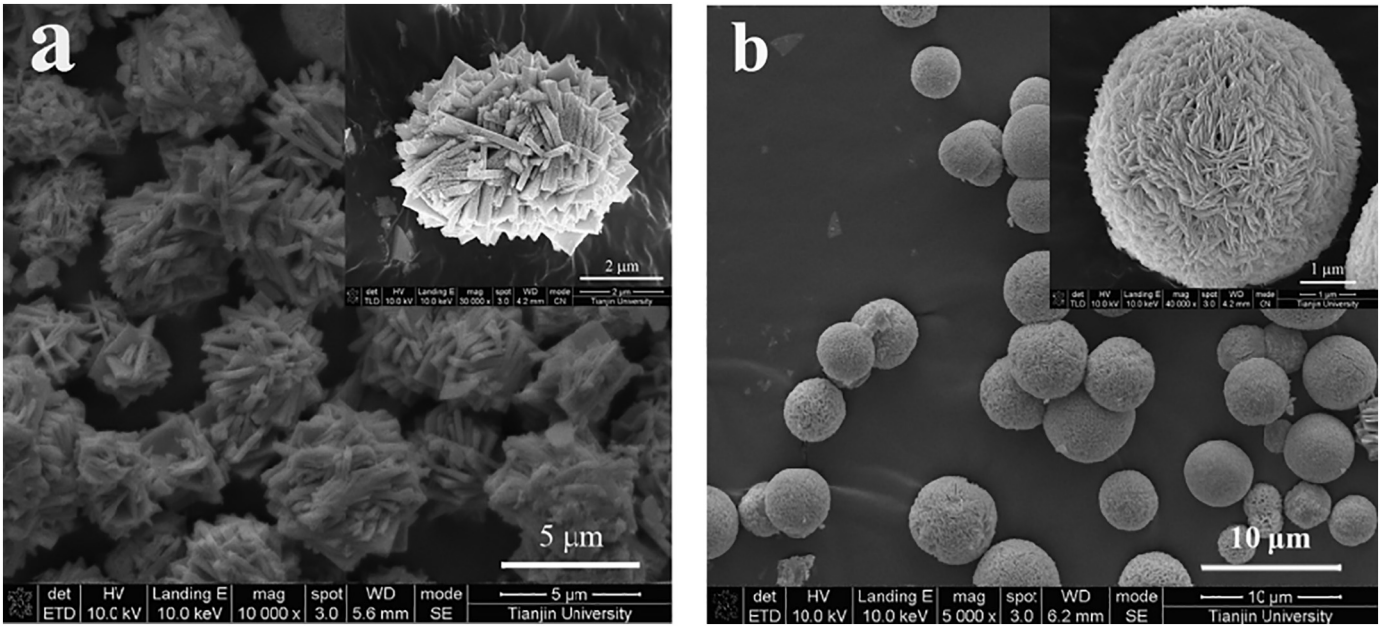

Fig. 5. SEM images of (a) flower-like BiOBr and (b) sphere-like BiOBr.
(Reprinted with permission from ref. [49]. Copyright (2015) Elsevier.)

photocatalysis occur on the surface of BiOX photocatalytic nanomaterials. And different facets possess different photocatalytic performance because of their different geometric and electronic structures [52,53]. Ye et al. [47] first prepared BiOCl nanosheets with tunable {001} crystal facets through hydrolyzing molecular precursor ($Bin(Tu)_xCl_{3n}$, Tu = thiourea). And they discovered that the main reactive facets of BiOCl crystals are the {001} facets. The enhanced photocatalytic activity could be attributable to the oxygen vacancies formed on the {001} facets. These oxygen vacancies can generate a defect state lying close to the bottom of the CB over the BiOCl photocatalyst, thus promoting the separation of photo-induced electron-hole pairs and then improving the photocatalytic activity of the BiOCl.

To further clarify facet-dependent photocatalytic properties, their group synthesized BiOI nanosheets with exposed active {001} (BiOI-001) and {100} (BiOI-100) crystal facets for CO_2 photoreduction by regulating the hydrothermal reaction time [54]. Under UV–vis irradiation, the production rate of CO and CH_4 over BiOI-001 were 5.18 μmol h^{-1} g^{-1} and 1.78 μmol h^{-1} g^{-1}, while they were only 1.52 μmol h^{-1} g^{-1} and 1.50 μmol h^{-1} g^{-1} could be generated by BiOI-100. The differences of IEF and CB position might lead to the photocatalytic activity difference between BiOI-001 and BiOI-100. The self-induced IEF of BiOI is perpendicular to {001} facets but parallel to {100} facets, thus the separation and migration of charge carriers are more favorable for BiOI-001 due to the shorter diffusion distance. Besides, because the CB level of BiOI-001 is higher than BiOI-100, the BiOI-001 possesses the higher reduction activity [54]. Therefore, both the IEF and CB position are in propitious to the photocatalysis of the BiOI-001.

Furthermore, Pan et al. [55] prepared two types of BiOI photocatalysts with exposed active {110} (BiOI-110) and {001} (BiOI-001) crystal facets by a facile hydrothermal method (Fig. 6). During bisphenol A (BPA) degradation, the BiOI-110 displayed higher photocatalytic activity because the adsorption energy of O_2 on the {110} facets (0.209 eV) was smaller than that on the {001} facets (0.656 eV). The results showed that BiOI-110 could generate more $\bullet O_2^-$, thus leading to enhanced visible light photocatalytic activity. Consequently, it can trap more electrons, which promotes the separation efficiency of photo-excited electron-hole pairs and results in generating more reactive oxygen species (ROS) related to electrons and holes [55]. In addition, between the two samples, only the BiOI-110 is able to produce •OH because BiOI-110 has a stronger oxidation potential than BiOI-001. Many other studies introduced the effect of crystal facets on photocatalytic activity of BiOX nanomaterials (Table 1), however, it is still difficult to develop the facets with high reactivity and expound underlying reaction mechanisms of different crystal facets [56].

The defects in the exposed facets of semiconductors can also enhance their photocatalytic activity by changing their electronic structures, recombination efficiency of charge carriers and surface properties [64–67]. In previous study, it has been found that the high photocatalytic activity of {001} facets of BiOCl originated from the oxygen vacancies which could improve the separation efficiency of electro-hole pairs [47]. During the CO_2 photoreduction experiment, the oxygen vacancies on BiOCl nanoplates not only improve their trapping capacity for CO_2, but also promote the separation of photo-induced electron-hole pairs, resulting in the considerable CO yield (1.01 μmol h^{-1} g^{-1}) under simulated solar light [68].

Recently, Wang et al. [69] successfully synthesized BiOBr nanosheets with plenty of surface oxygen vacancies on exposed {001} facets by using polybasic carboxylic acids as chelant. In comparison with the pristine BiOBr nanosheets, the MO degradation rate over BiOBr nanosheets with surface oxygen vacancies was 5.3 times higher than the pristine BiOBr nanosheets. The enhancement came from the surface oxygen vacancies which could trap electrons to form $O_2\bullet^-$ radicals and leave a large number of holes on the VB consequently. Except for oxygen vacancy, Xie et al. [70] found the $V''_{Bi}V_{\ddot{O}}V''_{Bi}$ triple vacancy associates on exposed active {001} facets of atomic scale BiOCl nanosheets. These triple vacancy associates not only strengthen the adsorption ability for cationic dye molecules through making the {001} facets negatively charged, but also promote the generation of more reductive photo-induced electrons by elevating the CBM position. Therefore, the ultrathin BiOCl nanosheets with $V''_{Bi}V_{\ddot{O}}V''_{Bi}$ vacancy associates exhibited 5 times higher solar-light-driven photocatalytic activity than ordinary BiOCl nanoplates for RhB degradation due to the synergetic promotions

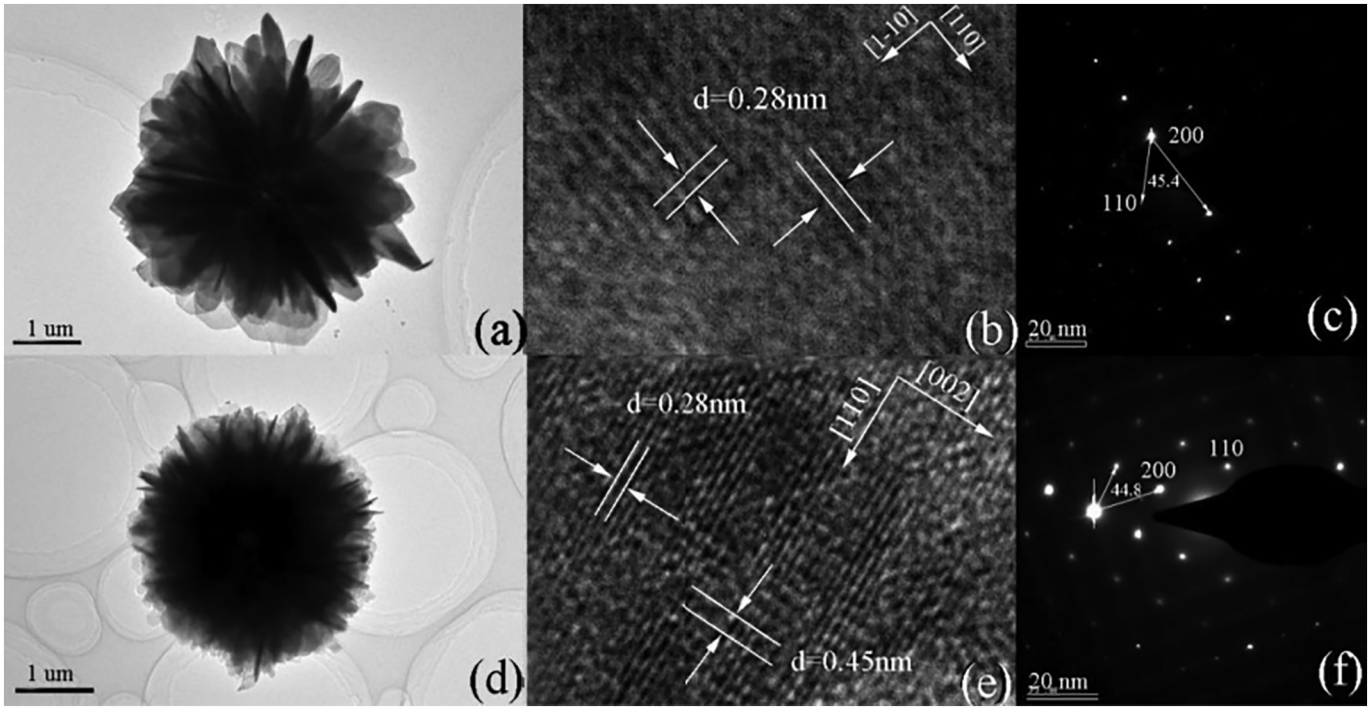

Fig. 6. (a) TEM, (b) HRTEM and (c) SAED images of BiOI-110. (d) TEM, (e) HRTEM and (f) SAED images of BiOI-001. (Reprinted with permission from ref. [55]. Copyright (2015) American Chemical Society.)

Table 1
Effects of exposed crystal facets on photocatalytic activity of BiOX nanomaterials.

Examples	Exposed facets	Synthetic methods	Facets control	Photocatalytic results	Ref.
BiOCl SCNSs	80% {001} facets 73% {010} facets	Hydrothermal	pH	Degradation efficiency of MO is 99% (UV, 45 min) and 10% (Vis, 180 min) Degradation efficiency of MO is 59% (UV, 45 min) and 33% (Vis, 180 min)	[44]
BiOCl NSs	0, 71%, 75% and 87% {001} facets	Hydrothermal	Feed ratios	Degradation efficiency of RhB is 9.6%, 33.6%, 48.1% and 81.1% (UV, 32 min)	[47]
Ag-BiOCl SCNSs	71% {001} facets 77% {010} facets	Microwave-assisted solvothermal (EG)	–	Removal efficiency of Cr(VI) and NaPCP are 65% and 63% (Vis, 180 min) Removal efficiency of Cr(VI) and NaPCP are 86% and 80% (Vis, 180 min)	[57]
g-C3N4/BiOCl	{001} facets {010} facets	Hydrothermal	pH	Degradation efficiency of MO and phenol are 65% and 40% (Vis, 150 min) Degradation efficiency of MO and phenol are 94% and 54% (Vis, 150 min)	[58]
C-doped BiOCl/NiO*x*	{001} facets {010} facets	Hydrothermal and impregnation method	pH	Photocatalytic H_2 evolution rate is 0.24 mmol h^{-1} g^{-1} (Vis) Photocatalytic H_2 evolution rate is 0.42 mmol h^{-1} g^{-1} (Vis)	[59]
Bi@BiOCl	{001} facets {010} facets	Hydrothermal	pH	Removal efficiency of NO is 35% (Vis, 30 min) Removal efficiency of NO is 50% (Vis, 30 min)	[60]
BiOBr NSs	{001} facets	Hydrothermal	pH	CO production rate is 4.45 μmol h^{-1} g^{-1} (UV–Vis, 2 h)	[38]
BiOBr NSs	{001} facets	Combustion	Amount of NH_4Br	Highest degradation efficiency of RhB is 91.6% (Vis, 120 min)	[45]
BiOBr NSs	94% {001} facets	Hydrolysis	Temperature and solvent	Degradation efficiency of RhB is 100% (Vis, 60 min)	[46]
BiOBr NSs	{102} facets {001} facets	Hydrothermal	Temperature and solvent	Degradation efficiency of RhB is 100% (Vis, 16 min) Degradation efficiency of RhB is 80% (Vis, 16 min)	[61]
BiOBr	{001} facets {110} facets	Hydrolysis Hydrothermal	–	Removal efficiency of Cr(VI) is 40% (Vis, 50 min) Removal efficiency of Cr(VI) is 100% (Vis, 50 min)	[62]
BiOI NSs	{001} facets {100} facets	Hydrothermal	Time	Production rate of CO and CH_4 are 5.18 μmol h^{-1} g^{-1} and 1.78 μmol h^{-1} g^{-1} (UV–Vis) Production rate of CO and CH_4 are 1.52 μmol h^{-1} g^{-1} and 1.50 μmol h^{-1} g^{-1} (UV–Vis)	[54]
BiOI MCSs	{001} facets {110} facets	Hydrothermal	Time	Degradation efficiency of BPA is 52%, TOC value decreased by 44% (Vis, 5 h) Degradation efficiency of BPA is 95%, TOC value decreased by 95% (Vis, 5 h)	[55]
BiOI MCSs	{001} facets	Solvothermal	–	Removal efficiency of RhB and Cr(VI) are 99% and 100% (Vis)	[63]

SCNSs: single-crystalline nanosheets; NSs: nanosheets; MCSs: microspheres.

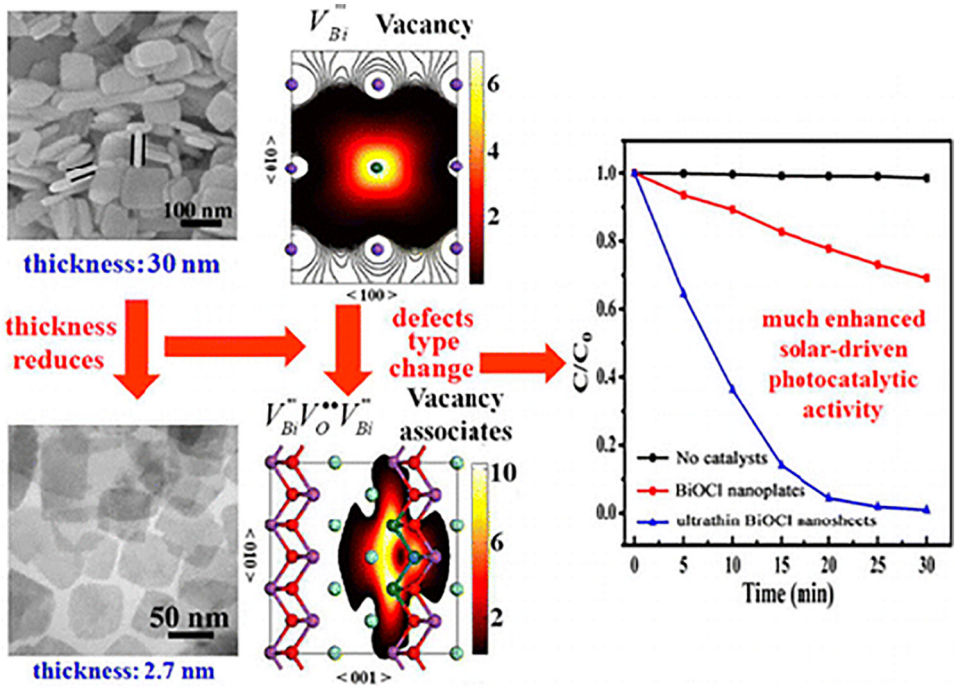

Fig. 7. Effect of BiOCl $V_{Bi}^{'''}V_{\dot{O}}V_{Bi}^{'''}$ formation on photocatalytic activity.
(Reprinted with permission from ref. [70]. Copyright (2013) American Chemical Society.)

of improved adsorption ability, effective separation of photo-induced electron-hole pairs and more reductive photo-generated electrons (Fig. 7).

However, the oxygen vacancy doesn't always play a positive role in photocatalytic reactions. Chen et al. [71] synthesized BiOCl nanoplates with exposed active {001} crystal facets through a simple hydrothermal method. Because oxygen vacancy can be easily formed under UV light irradiation, they found that the as-prepared samples exhibited about 3 times higher rate constant (k) for photocatalytic degradation of RhB under visible light (0.034 min^{-1}) than that under UV–vis light irradiation (0.012 min^{-1}). The photosensitization is the main way for BiOCl nanosheets to degrade RhB under visible light irradiation. In contrast, oxygen vacancies are formed on {001} facets of BiOCl nanosheets under UV–vis light irradiation and they can hinder the generation of $\bullet O_2^-$ radicals by trapping photo-induced electrons on the CB of BiOCl. Hence, oxygen vacancies in BiOCl nanosheets here reduce the photocatalytic degradation efficiency of RhB.

3.3. Carbonaceous materials compounding

Various carbonaceous materials, including graphene, carbon nanotubes (CNTs), carbon quantum dots (CQDs) and biochar, play important roles in enhancing photocatalytic performance of BiOX nanomaterials. Graphene (usually refers to reduced graphene oxide (RGO)) has been considered as a good electron collector and transporter in photocatalysis because of its high conductivity, excellent electron mobility and large specific surface area [16,72–74]. Based on those results, RGO/BiOX nanocomposites exhibit significantly enhanced photocatalytic activity [75–77]. Recently, Dong et al. [75] synthesized flower-like BiOCl/RGO nanocomposites to degrade sulfanilamide (SN) under natural sunlight irradiation. And the samples contained 1 wt% RGO showed excellent photocatalytic activity due to the improved electron transfer ability and enhanced visible light absorption, rather than the changes of surface area value and band gap.

CNTs are used for photocatalysis owing to their excellent ability to conduct electrons [78]. Very recently, CNTs have been used in some CNT/BiOX nanocomposites to increase the separation efficiency of photo-excited electron-hole pairs, and thus enhancing the photocatalytic activity [79–81]. S. Vadivel et al. [79] synthesized multiwall carbon nanotubes (MWCNT)/BiOCl nanocomposites via one step hydrothermal approach. The as-obtained samples showed superior photocatalytic activity in photodegradation of congo red, malachite green and bromophenol blue dyes than pure BiOCl, and the improved photo-generated electron-hole pairs separation efficiency was the predominant reason. As new carbonaceous nanomaterials, CQDs have been also extensively applied in photocatalytic applications relied on their superior electron transfer ability [82]. A series of CODs/BiOX nanomaterials have been synthesized [83–86], for example, Xia et al. [84] obtained a range of CQDs/BiOX (X = Cl, Br) nanosheets with different CQDs contents by ionic liquid-assisted hydrothermal method (Fig. 8). Due to their high visible light absorbance, enhanced separation efficiency of photo-generated electron-hole pairs and lower resistance, the 3 wt% CQDs/BiOBr nanosheets exhibited the optimal catalytic efficiency for the degradation of RhB, ciprofloxacin (CIP) and BPA. However, abovementioned carbonaceous nanomaterials suffer from some deficiencies, such as complex synthesis method and high cost. Therefore, biochar, an easily accessible and low cost carbonaceous material, has entered people's field of vision [87,88]. Li et al. [89] first utilized biochar to produce biochar/BiOX (X = Cl, Br) photocatalysts through a facile in-situ precipitation method. And they found that biochar could act as a benign carrier of electrons to promote photocatalytic reactions for BiOBr and photosensitization reactions for BiOCl.

3.4. Heterojunction construction

Heterojunction construction is the most common strategy to enhance the photocatalytic performance of a single semiconductor, which can accelerate the separation of photo-induced carriers and broaden the wavelength of photo-response for the system [90]. Our team fabricated a Bi/BiOCl/$ZnSn(OH)_6$ heterojunction and investigated its photocatalytic activity by RhB degradation under visible light irradiation [25]. The photo-degradation rate of RhB over Bi/BiOCl/$ZnSn(OH)_6$

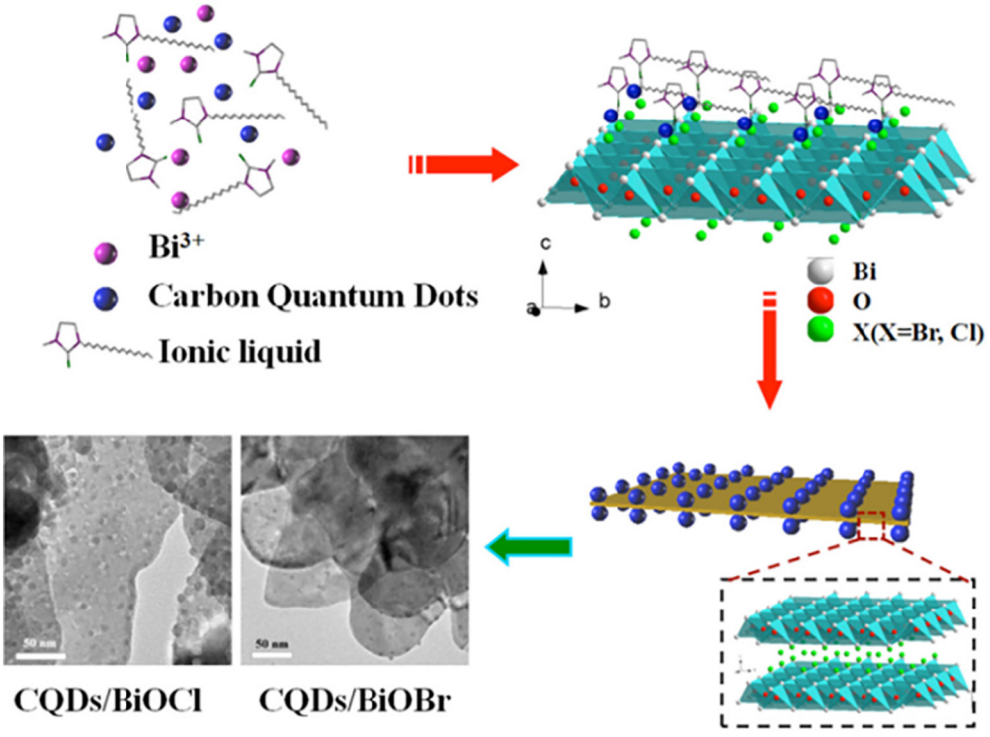

Fig. 8. Diagram of the synthetic procedure for CQDs/BiOX hybrid nanosheets.
(Reprinted with permission from ref. [84]. Copyright (2015) Elsevier.)

was about 81 times higher than that of pure $ZnSn(OH)_6$, demonstrating that the combination of $ZnSn(OH)_6$ with Bi and BiOCl was an advisable method. The addition of Bi nanoparticles and BiOCl nanosheets not only extend the range of absorption wavelength to visible light from light region, but also promote the separation of charge carriers by the formation of heterojunction among different components.

In recent work, Li et al. [58] constructed g-C_3N_4/BiOCl heterostructures where nanosized g-C_3N_4 (ng-CN) is loaded in different exposed crystal facets ({001} and {010}) of BiOCl nanosheets (BOC-001 and BOC-010). Because of the existence of IEF, as shown in Fig. 9, photo-generated electrons transferring from ng-CN to the reactive site of BiOCl nanosheets had a longer migratory distance in BOC-001 than that in BOC-010, leading to the loss of more electrons. These two samples showed significantly improved MO and phenol photodegradation ability under visible light, and the ng-CN/BOC-010 heterojunction exhibited better photocatalytic performance than the ng-CN/BOC-001 heterojunction. This research suggests that the orientation of different exposed facet in semiconductors is a new direction for constructing high-performance heterojunction photocatalysts. Besides, other heterojunction photocatalysts, such as $Bi_2O_2CO_3$/BiOCl [91], BiOI/CdS [92], BiOBr/MoS_2 [93], Bi_2WO_6/BiOI [94], BiOBr/$ZnFe_2O_4$ [95], $CoTiO_3$/BiOBr [96], BiOCl/TiO_2 [97], Fe_3O_4/BiOI [98], WO_3/BiOI [99] and $NaBiO_3$/BiOCl [100] have been developed and were confirmed to be excellent VLD photocatalysts.

3.5. Other strategies

Up to date, the limited visible light absorption and short photo-induced electron-hole pair lifetimes are still two major factors restricting the practical application of semiconductor photocatalysts. To strengthen the VLD photocatalytic activity of BiOX photocatalysts, solid solutions, doping and bismuth-rich strategy are also feasible methods. The generation of solid solutions can narrow their energy band gap through lifting the position of VB and/or lowering the position of CB, which can improve their photocatalytic abilities [101]. Until now, a lot of BiOX solid solution photocatalysts with enhanced VLD photocatalytic activities have been prepared, such as $BiOCl_{1-x}Br_x$ [102], $BiOBr_{1-x}I_x$ [103], $BiOCl_{1-x}I_x$ [104], $(BiO)_2(CO_3)_x(I_2)_{1-x}$ [105] etc. Different from the formation of solid solutions, doping often introduce a foreign element into the host materials, which leads to dispersed energy levels above VB or below CB. This can efficient trap photo-generated electrons and decrease band gap [106]. Therefore, a series of non-metal (e.g., C, N, F) [107–109] and metal (e.g., Fe, Zn, Sn) [110–112] elements have been doped into BiOX photocatalytic nanomaterials recently and the doped nanomaterials exhibit superior VLD photocatalytic activity than the single sample. The bismuth-rich strategy can uplift the CB potential through changing the bismuth content, because the CB of BiOX photocatalysts is mainly consisted of Bi 6p state [113]. It has been reported that $Bi_{24}O_{31}Br_{10}$ [113], $Bi_4O_5Br_2$ [114] and Bi_4O_5BrI [115] all have increased CBM potential as well as photocatalytic reduction enhancement.

Owing to those mentioned strategies, the form of BiOX photocatalytic nanomaterials are changed from single materials to modified complex nanomaterials and the VLD photocatalytic capacities of BiOX photocatalysts are greatly improved. These allow BiOX photocatalysts to adapt to a wider range of applications, especially in the fuels preparation from H_2O and CO_2 (Table 2), removal of heavy metals and air pollutants, as described in the following sections.

4. BiOX nanomaterials to make fuels from H_2O and CO_2

4.1. Photocatalytic hydrogen generation

Photocatalytic water into H_2 and O_2 is perhaps the most urgent task of present research for solving the energy and environmental problems. Although the CB potential of BiOX can't satisfy the reduction potential of H^+ to H_2, recent researches clearly corroborated that H_2 production on BiOX can be achieved by forming heterojunction [120,126], introducing cocatalysts [117], coupling photosensitizers [116], doping foreign elements [59], tailoring crystal facets [59,117,118], utilizing defects [116,118,119,127,128], applying strains [129] and reducing thickness [118,127,130]. For example, Ye et al. [118] prepared black ultrathin BiOCl nanosheet (BU-BiOCl) which has expanded {001} facet spacing and abundant oxygen vacancies (Fig. 10a and b). The expanded facets spacing can strengthen the IEF intensity and finally promote the separation of photo-induced carriers. Results in Fig. 10c show that BU-BiOCl has more H_2 production (2.51 μmol h^{-1}) than bulk BiOCl (0.12 μmol h^{-1}) under visible light irradiation. After loading Pt, BU-BiOCl/Pt also displays superior photocatalytic activity for H_2 production (3.96 μmol h^{-1}) than bulk BiOCl/Pt (0.18 μmol h^{-1}). These results indicate that oxygen vacancies and expanded {001} facets spacing can improve the photocatalytic activity significantly, which can be attributed to the enhanced photon absorption efficiency and separation efficiency of photo-excited carriers.

Recently, Zhang and co-workers [59] developed BiOCl nanosheets with carbon doped in {001} and {010} facet and applied it to H_2 production with the help of NiO_x co-catalyst and hole scavenger triethanolamine (TEOA). Carbon-doped BiOCl nanosheets with 3 wt%

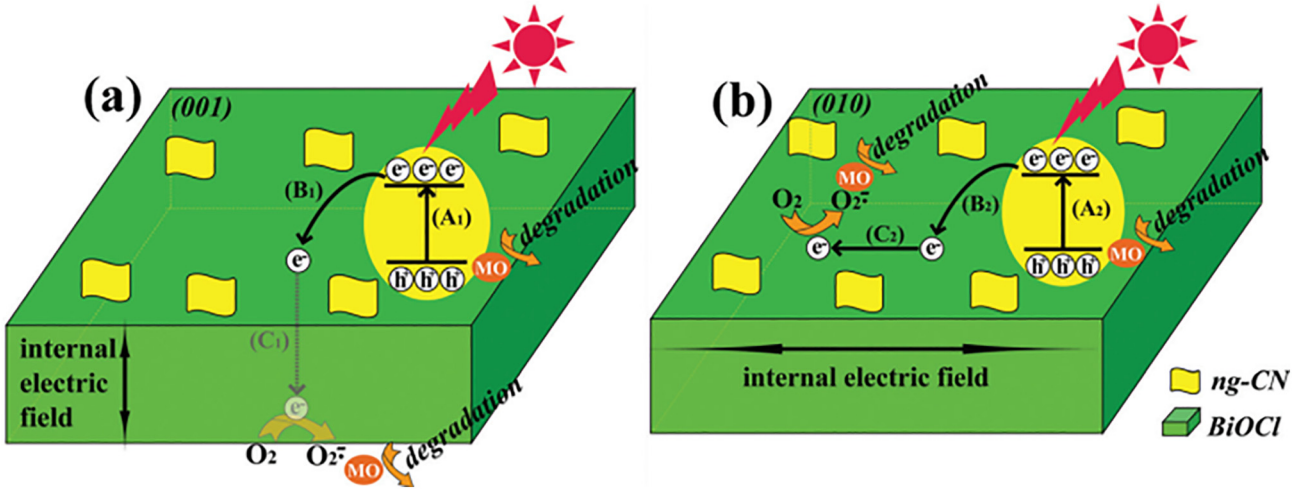

Fig. 9. Photocatalytic reaction mechanism of (a) ng-CN/BOC-001 and (b) ng-CN/BOC-010.
(Reprinted with permission from ref. [58]. Copyright (2015) The Royal Society of Chemistry.)

Table 2
Recent studies on BiOX (X = Cl, Br, I) photocatalytic nanomaterials used for fuels preparation from H_2O and CO_2.

Photocatalytic applications	Examples	Synthetic methods	Light	Photocatalytic activity	Ref.
Water splitting to H_2	Carbon-doped BiOCl/NiO_X	Hydrothermal carbonization, thermal-induced doping and impregnation	500 W Xe lamp	0.42 mmol h^{-1} g^{-1} H_2	[59]
	BiOCl/CuPc	Solvothermal synthesis(EG)	500 W Xe lamp	20 μmol h^{-1} g^{-1} H_2	[116]
	BiOCl@Au/MnOx	Hydrothermal synthesis and photodeposition	500 W Xe lamp	66 μmol h^{-1} g^{-1} H_2	[117]
	BU-BiOCl/Pt	Solvothermal synthesis (glycerol)	300 W Xe lamp λ > 420 nm	79.2 μmol h^{-1} g^{-1} H_2	[118]
	$Bi_{12}O_{17}Cl_2/MoS_2$	Chemical liquid exfoliation	300 W Xe lamp λ > 420 nm	33 mmol h^{-1} g^{-1} H_2	[119]
	BiOBr/α-Fe_2O_3/Pt	Hydrothermal synthesis	300 W Xe lamp λ > 420 nm	16.08 μmol h^{-1} g^{-1} H_2	[120]
Reduction of CO_2 to fuels	Oxygen-deficient BiOCl nanoplates	Solvothermal synthesis(EG)	500 W Xe lamp	1.01 μmol h^{-1} g^{-1} CO, 0.15 μmol h^{-1} g^{-1} CH_4	[68]
	BiOBr-001 nanosheets	Hydrothermal synthesis	300 W Xe lamp	4.45 μmol h^{-1} g^{-1} CO	[38]
	BiOBr	Solvothermal synthesis (ethanol)	300 W Xe lamp λ > 400 nm	1.68 μmol h^{-1} g^{-1} CO, 0.17 μmol h^{-1} g^{-1} CH_4	[114]
	Ultrathin BiOBr	Solvothermal synthesis (ethanol)	300 W Xe lamp λ > 400 nm	2.67 μmol h^{-1} g^{-1} CO, 0.16 μmol h^{-1} g^{-1} CH_4	[114]
	$Bi_4O_5Br_2$ microspheres	Solvothermal synthesis (glycerol) and hydrolysis	300 W Xe lamp λ > 400 nm	2.73 μmol h^{-1} g^{-1} CO, 2.04 μmol h^{-1} g^{-1} CH_4	[114]
	Bi_2O_4/BiOBr	Hydrothermal synthesis	300 W Xe lamp	2.60 μmol h^{-1} g^{-1} CO, 1.85 μmol h^{-1} g^{-1} CH_4	[121]
	Oxygen-deficient BiOBr	Solvothermal synthesis(EG)	500 W Xe lamp 500 W Xe lamp λ > 400 nm	0.96 μmol h^{-1} g^{-1} CH_4 0.49 μmol h^{-1} g^{-1} CH_4	[122]
	BiOI-001 nanosheets	Solvothermal synthesis (ethanol)	300 W Xe lamp	5.18 μmol h^{-1} g^{-1} CO, 1.78 μmol h^{-1} g^{-1} CH_4	[54]
	BiOI-100 nanosheets	Solvothermal synthesis (ethanol)	300 W Xe lamp	1.52 μmol h^{-1} g^{-1} CO, 1.50 μmol h^{-1} g^{-1} CH_4	[54]
	Au/BiOI/MnO_X	Photodeposition	300 W Xe lamp 300 W Xe lamp λ > 420 nm	42.9 μmol h^{-1} g^{-1} CO, 1.36 μmol h^{-1} g^{-1} CH_4 9.76 μmol h^{-1} g^{-1} CO, 0.39 μmol h^{-1} g^{-1} CH_4	[123]
	Few-layered BiOI	Solvothermal synthesis(EG)	300 W Xe lamp λ > 420 nm 300 W Xe lamp λ > 700 nm	4.10 μmol h^{-1} g^{-1} CO, 0.42 μmol h^{-1} g^{-1} CH_4 0.80 μmol h^{-1} g^{-1} CO, 0.14 μmol h^{-1} g^{-1} CH_4	[124]
	BiOI/g-C_3N_4	Deposition	300 W Xe lamp λ > 400 nm	3.45 μmol h^{-1} g^{-1} CO, 0.16 μmol h^{-1} g^{-1} CH_4, 0.37 μmol h^{-1} g^{-1} H_2	[125]

NiO_x loading on {010} facet (BOC-010HC) exhibited the highest photocatalytic H_2 evolution rate (0.42 mmol h^{-1} g^{-1}) due to the increased optical absorption efficiency and enhanced IEF intensity [59,119]. However, in this experiment, as a result of the moderate IEF intensity and random distribution of NiO_x, H_2 production rate is still very low [59]. In order to overcome these shortcomings, their team gained oxygen vacancy-rich $Bi_{12}O_{17}Cl_2$ monolayer nanosheets assembled with metallic MoS_2 monolayers by chemical liquid exfoliation method [119,131]. Such a Janus bilayer construction endows atomic-level control over carrier separation, transportation and consumption, thus achieving a spectacular photocatalytic H_2 production rate (33 mmol h^{-1} g^{-1}) under visible light irradiation.

These results definitely demonstrate the feasibility of the BiOX photocatalysts for H_2 production under visible light with the help of some strategies. Although their yield of hydrogen could not meet the practical production needs now, the potential of BiOX nanomaterials for producing H_2 is tremendous in view of following aspects. Firstly, their CBM is close to the reduction potential of H^+/H_2, and can be easily lifted to beyond it. Secondly, the layered structures of BiOX can motivate an IEF which is capable of efficient separation and migration of photogenerated electron-hole pairs. Thirdly, their internal strain differences and oxygen termination feature bring the easy generation of oxygen vacancies [119,129].

4.2. Photocatalytic reduction of carbon dioxide

As a result of the increasing use of fossil fuels, CO_2 has caused much attention as a greenhouse gas, and now has been deduced into a serious environmental problem. Converting CO_2 into the energy-bearing carbon fuel sources by photocatalytic reduction is undoubtedly one of the most economical and sustainable methods to reduce levels of CO_2 in the atmosphere and solve energy problems [132–134]. However, the application of BiOX in the field of CO_2 conversion is very limited due to their relatively positive CB position and weak reduction power. The photocatalytic reduction abilities rely on the CBM position, therefore, some strategies adopted to tune the CBM position of BiOX for enhancing the efficiency of CO_2 conversion, such as morphology control [48,114], defect effect [68,122], cocatalyst [121,123], crystal facet control [38,54,124], heterojunction [125,135] and bismuth-rich strategy [114].

In 2016, Kong and co-workers [122] reported an oxygen-deficiency method for BiOBr nanosheets for improved photocatalytic reduction activity. In their study, oxygen-deficient BiOBr nanosheets with oxygen vacancies were fabricated through an ethylene glycol-assisted solvothermal process. The as-prepared BiOBr nanosheets exhibited a huge improvement for CH_4 production under visible light irradiation, obtaining a total yield of 4.86 μmol g^{-1}, while the pristine BiOBr only achieved 1.58 μmol g^{-1} of CH_4. Especially, oxygen-deficient BiOBr nanosheets showed a 9.58 μmol g^{-1} of CH_4 formation yield under simulated solar light irradiation, which was 3.2 and 5.7 times higher than that of pristine BiOBr and Degussa P25, respectively.

Considering that the band gap energy of oxygen-deficient BiOBr nanosheets (2.70 eV) is very close to the pristine BiOBr (2.85 eV), the enhanced production of fuels could mainly be ascribed to several factors as follows: Firstly, the oxygen-deficient surface highly improves the optical properties of BiOBr and promotes electron-hole pair generation by enhancing light absorption; secondly, oxygen vacancies can trap photo-induced electrons, thus promoting the electron-hole pair separation and restraining the recombination of charge carriers; thirdly, the adsorbed CO_2 molecules and oxygen vacancies probably generate

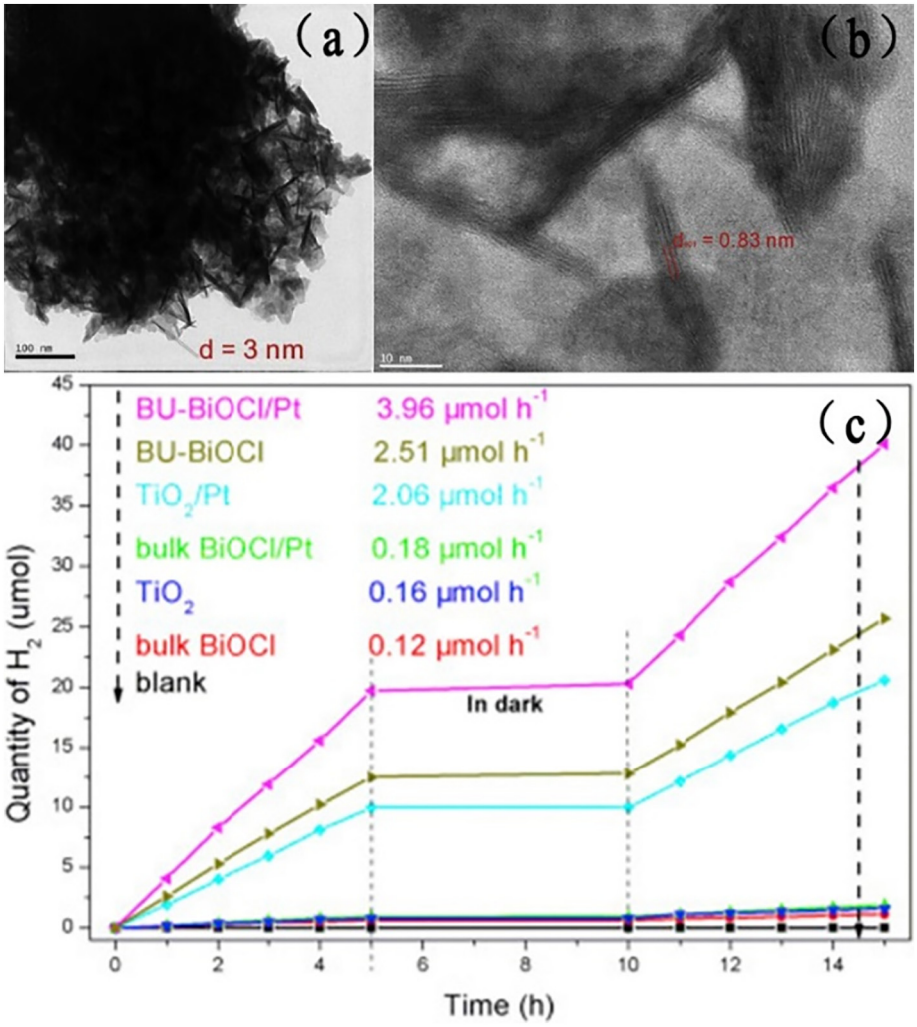

Fig. 10. (a, b) HRTEM images of BU-BiOCl. (c) Yields of H_2 over TiO_2, bulk BiOCl, BU-BiOCl, TiO_2/Pt, bulk BiOCl/Pt and BU-BiOCl/Pt under visible light irradiation. (Reprinted with permission from ref. [118]. Copyright (2015) Elsevier.)

unexpected interactions, which can accelerate the interfacial charge transfer [122].

The use of cocatalysts is another significant method to improve the photocatalytic activity of BiOX for the reduction of CO_2 into solar fuels. In 2016, Bai and co-workers [123] prepared a dual-cocatalyst-loaded Au/BiOI/MnOx photocatalyst for CO_2 reduction (Fig. 11a–d). Under UV–vis light irradiation, the CO production rate of Au/BiOI/MnO_x sample was 42.9 μmol h^{-1} g^{-1}, which was about 7.0 times higher than that of bare BiOI (6.12 μmol h^{-1} g^{-1}). Under visible light irradiation, the CO production rate increased from 0.51 μmol h^{-1} g^{-1} for pure BiOI to 9.76 μmol h^{-1} g^{-1} for the Au/BiOI/MnO_x sample (Fig. 11e). Finally, the total yields of CO reached 169 μmol g^{-1} in the presence of Au/BiOI/MnO_x after 5 h of photocatalytic reaction (Fig. 11f) [123]. This enhancement could be assigned to the cocatalysts including Au and MnO_x because they can't only act as redox-active sites but also improve the separation efficiency of photo-induced charge carriers. Firstly, Au nanoparticles and MnO_x layers are loaded on BiOI nanosheets with photo-excitation. Next, the photo-generated electrons and holes can transfer to the Au and MnO_x respectively and this transfer process can restrain the recombination of the photo-excited electron-hole pairs. Lastly, the photo-excited electrons can be used for CO_2 reduction.

Over past decades, some significant advances in CO_2 conversion by using BiOX photocatalytic nanomaterials have been achieved. However, the relatively low yields and selectivity of the desired products resulting from the complex processes and kinetics of CO_2 photoreduction still hinder the practical application. In view of practical utilization, all the factors (e.g., excitation, separation and migration of charge carriers, adsorption of CO_2 and CO_2 reduction kinetics) should be considered and optimized when designing and synthesizing BiOX photocatalytic nanomaterials for CO_2 reduction.

5. BiOX nanomaterials for environmental managenemt

5.1. Photocatalytic degradation of organic pollutants

In recent years, a lot of effort has been devoted to treating the varied organic pollutants which come from domestic, industrial and medical effluents [136–141]. Various nanomaterials have been extensively applied in the removal of organic pollutants [26,142–144]. Among them, BiOX nanomaterials have many unusual properties which endow them excellent photocatalytic activities, such as open layered structures, indirect optical transition and high surface-to-volume ratio [30,39]. Therefore, BiOX photocatalytic nanomaterials have been widely used for refractory organic pollutants decomposition. For example, Hao et al. [145] synthesized microsphere-like BiOI hierarchical nanomaterial through a one-step solution process at room temperature and utilized it to remove tetracycline hydrochloride (TC). After 2 h visible light irradiation, the TC removal efficiency by BiOI microspheres reached 94%, while only 44% TC could be degraded over the BiOI nanoplatelets,

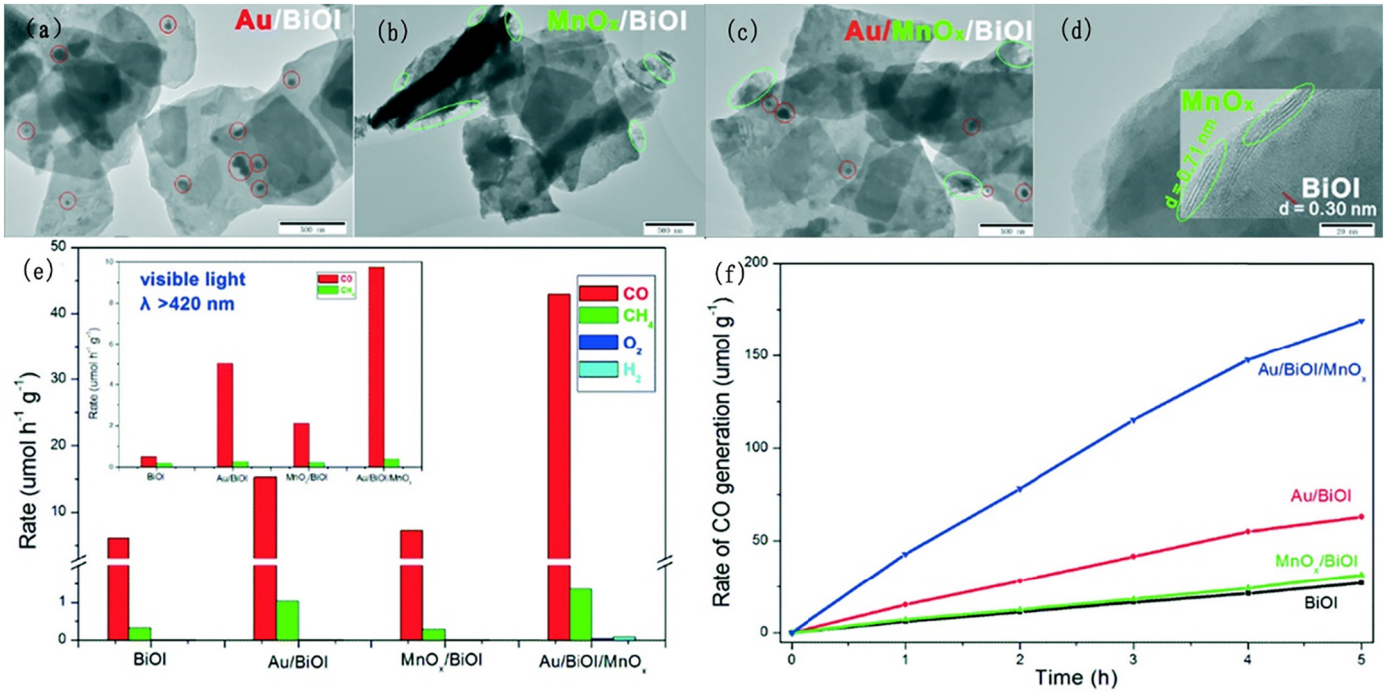

Fig. 11. TEM images of (a) Au/BiOI, (b) MnOx/BiOI, (c and d) Au/BiOI/MnOx. (e) Rates of products over BiOI, Au/BiOI/MnOx, Au/BiOI, and MnOx/BiOI under UV–vis light irradiation (the inset displays the corresponding rates of products under visible light irradiation). (f) CO yields on BiOI, Au/BiOI/MnOx, Au/BiOI, and MnOx/BiOI for 5 h under UV–vis light irradiation. (Reprinted with permission from ref. [123]. Copyright (2016) The Royal Society of Chemistry).

and by comparison, the removal of TC on BiOI microspheres was only 40% in the darkness. Several reasons could be concluded for the excellent removal capability of BiOI microspheres, such as energy band structure, large BET surface area and high surface-to-volume ratio [145].

The photocatalysis process is considered to be the main pathway for the removal of organic pollutants by BiOX nanomaterials. In order to further enhance their ability to photocatalytic degradation of organic pollutants under visible light, several strategies have been developed [146–149]. Recently, Di et al. [146] reported that graphene-like boron nitride (BN) modified BiOBr flower-like nanomaterials showed satisfying photocatalytic activity for the degradation of CIP, TC and RhB. This enhancement is attributed to the decoration of BN, which could improve the visible light harvesting ability and facilitate the separation of photo-generated electron-hole pairs.

Especially, constructing efficient BiOX-based nanocomposites for organic pollutants removal often requires the synergetic effect of several

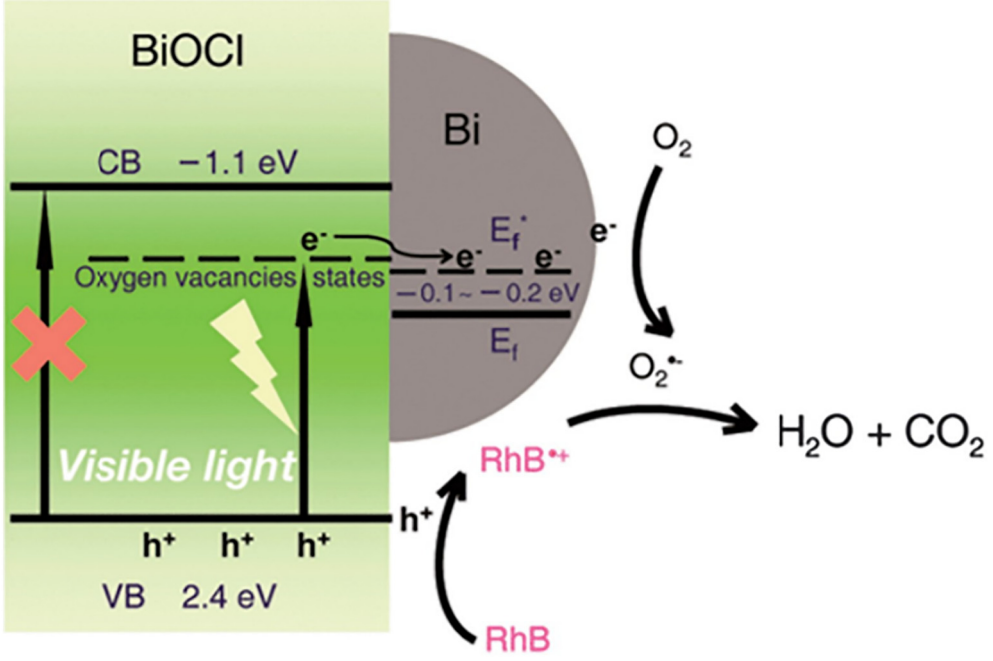

Fig. 12. Photocatalytic mechanism diagram of oxygen vacancies modified Bi/BiOCl heterojunction photocatalysts under visible light irradiation. (Reprinted with permission from ref. [147]. Copyright (2014) The Royal Society of Chemistry.)

systems [33]. Yu et al. [147] demonstrated that Bi/BiOCl heterojunction with oxygen vacancies exhibited outstanding photodegradation activity for dyes and persistent organic pollutants under visible light. This is mainly due to the fact that the abundant oxygen vacancies on BiOCl photocatalyst narrow its band gap to the visible light range and the formed Bi nanoparticles on the BiOCl surface accelerate the transfer of photo-induced electrons from BiOCl to Bi. $\bullet O_2^-$ and photo-induced holes are proved to be the main active species in this photocatalytic degradation process [147]. The reaction mechanism is shown in Fig. 12, which reveals that organic pollutant molecules can react with active holes on the VB of the BiOCl to form radical ions and then react with $\bullet O_2^-$ to form the final inorganic products. Moreover, I-BiOCl/I-BiOBr composite combined the merits of I^- ion doping and BiOCl/BiOCl heterojunction, exhibiting largely enhanced photocatalytic activities for the degradation of MO and phenol under visible light [148]. The result shows that the synergistic effect of doping and heterojunction is the key for the excellent photocatalytic activity of the I-BiOCl/I-BiOBr composite.

In most of reactions that utilize BiOX photocatalysts to degrade organic pollutants, photo-induced holes and $\bullet O_2^-$ radicals are considered to be the dominant reactive species [146,147,150]. Xiao et al. [151] found that photo-induced holes and $\bullet O_2^-$ radicals played key roles in the BPA degradation experiment by BiOI. The photo-induced holes of BiOX photocatalysts cannot react with H_2O/OH^- to form •OH radicals because the standard redox potential of Bi(V)/Bi(III) (+1.59 V) is lower than that of $\bullet OH/OH^-$ (+1.99 V) [152]. Besides, some studies demonstrate that •OH and photo-induced holes are the two primary reactive species in photocatalysis [153]. Gao et al. [98] fabricated high-performance 3D hollow magnetic Fe_3O_4/BiOI heterojunction for removal of BPA under visible light. The radical trapping experiments proved that photo-generated holes and •OH were the main active species in the Fe_3O_4/BiOI system. The •OH originated from the reduction of O_2: the photo-generated electrons reacted with the adsorbed O_2 to generate $\bullet O_2^-$ and subsequently H_2O_2; H_2O_2 reacted with an electron and generated •OH. The detailed photocatalytic process of Fe_3O_4/BiOI system was displayed as below [98].

$$Fe_3O_4/BiOI\ (hv) \rightarrow Fe_3O_4/BiOI\ (h^+ + e^-) \quad (1)$$

$$e^- + O_2 \rightarrow {}^{\cdot}O_2^- \quad (2)$$

$$2{}^{\cdot}O_2^- + 2H^+ \rightarrow O_2 + H_2O_2 \quad (3)$$

$$H_2O_2 + e^- \rightarrow OH^- + {}^{\cdot}OH \quad (4)$$

$$BPA + (h^+, {}^{\cdot}OH, {}^{\cdot}O_2^-) \rightarrow \text{degradation products} \rightarrow CO_2 + H_2O \quad (5)$$

However, many studies have focused on the photocatalytic degradation ability of BiOX nanomaterials, the adsorption ability of BiOX nanomaterials have been neglected to a great extent [146,148]. To clarify the effect of adsorption in BiOBr photocatalysis, Li and co-workers [154] prepared BiOBr microspheres for the ibuprofen (IBP) removal. In the adsorption process, the IBP and total organic carbon (TOC) removal rate were about 65% and 52%, respectively. While during the photocatalysis process, the removal rate increased slightly, were 80% and 63% accordingly. The small difference of removal percentage over IBP between adsorption and photocatalysis reaction indicates that most of the removal contribution is from adsorption of BiOBr microspheres. This demonstrates that the photocatalytic removal efficiency of IBP through BiOBr microspheres is highly adsorptivity dependent. And the better adsorption ability of the prepared catalysts could also facilitate the higher photocatalytic performance. Besides, they found that the ion exchange between bromide ion and dissociated IBP as well as the formation of O—Bi—O bond are the primary acting forces during the IBP removal process [154]. Meanwhile, Xu et al. [155] reported that the introduction of TiO_2 nanoparticles could tune the morphology, surface charge property, BET surface area, and hydrophilic property of layered BiOCl nanostructures and hence improve its adsorption ability towards Congo red.

5.2. Photocatalytic reduction of heavy metals

Unlike organic pollutants, heavy metals reduction is a tricky process and tend to accumulate in organisms and certain heavy metal ions are proved to be toxic or carcinogenic [156,157]. Conventional technologies for heavy metals removal mainly involve chemical precipitation, ion exchange, biological treatment and physical adsorption [158–162]. Compared with these methods, photocatalytic reduction has been regarded as an economic procedure, where the energy consumption was lowest and no secondary pollution could be brought out. The photocatalytic reduction process includes adsorption and reduction of heavy metal ions on the surface of the photocatalysts. Then the reduced metal can be removed by physical and/or chemical methods. Although BiOX nanomaterials as visible light photocatalysts have been mainly used for photo-degradation of organic pollutants, recent studies indicate that they have great potential for photoreduction of heavy metal ions.

M. Qamar and co-workers [163] first utilized BiOCl for the photocatalytic reduction of Cr(VI) and they found that BiOCl exhibited higher photocatalytic activity than Degussa P25 for Cr(VI) reduction. 95% and 49% Cr(VI) are reduced within short time (30 min) under 355 nm laser irradiation in presence of BiOCl and Degussa P25, respectively. However, the excellent photocatalytic efficiency may be attributed to the laser which is a strong, monochromatic and coherent source of light [163]. Therefore, many methods have been applied so as to improve the capacity of BiOX nanomaterials to handle the toxic heavy metal under visible light.

Shang et al. [113] reported that BiOBr can be transformed into $Bi_{24}O_{31}Br_{10}$ with enhanced photocatalytic reduction activity through a bismuth-rich strategy. In the experiment of photocatalytic reduction of Cr (VI) under visible light, $Bi_{24}O_{31}Br_{10}$ presents the highest ability among Bi_2O_3, BiOBr and $Bi_{24}O_{31}Br_{10}$, and Cr (VI) ions could be completely reduced in 40 min irradiation. Compared with BiOBr, $Bi_{24}O_{31}Br_{10}$ has uplifted CB level which attributed to the hybridization of Bi 6p states and Br 4 s states. Recently, Bai et al. [115] prepared solid solutions of bismuth-rich $Bi_4O_5Br_xI_{2-x}$ by the molecular precursor method and utilized it for photocatalytic Cr(VI) removal under visible light irradiation. The Cr(VI) removal ratios of $Bi_4O_5Br_2$, Bi_4O_5BrI and $Bi_4O_5I_2$ are 47%, 88% and 53%, this means that Bi_4O_5BrI solid solutions exhibit much better photocatalytic reduction ability for Cr(VI) removal than $Bi_4O_5Br_2$ and $Bi_4O_5I_2$. This enhancement is ascribed to the higher CB position and faster photo-induced carrier separation rates endowed by solid solution strategy and bismuth-rich method [115]. This work indicates that synergistic effect of solid solutions and bismuth-rich could significantly enhance the efficiency of BiOX photocatalysts for Cr(VI) removal.

The pH of the initial solution usually affects the photoreduction of the heavy metals [142]. Very recently, Xu and co-workers [164] fabricated BN-doped BiOCl nanocomposites with flower-like microsphere structure through a facile microwave-assisted method for the removal of Cr(VI) contaminants. The FESEM and HRTEM of 1% BN/BiOCl composite are displayed in Fig. 13a and b, respectively [164]. Under acidic conditions, the surface of BN/BiOCl adsorbs a great deal of H^+, which can not only give access to protonation but also promote the accumulation of negatively Cr(VI) species such as $Cr_2O_7^{2-}$ and $HCrO_4^-$. Under alkaline conditions, the negative BN/BiOCl surface can only adsorb a little Cr (VI) because Cr(VI) species are exist as $Cr_2O_7^{2-}$. Moreover, the generated $Cr(OH)_3$ sediments restrain the photocatalytic activity of BN/BiOCl composite by blocking its active sites.

For acidic Cr(VI) solutions:

$$Cr_2O_7^{2-} + 14H^+ + 6e^- \rightarrow 2Cr^{3+} + 7H_2O \quad (6)$$

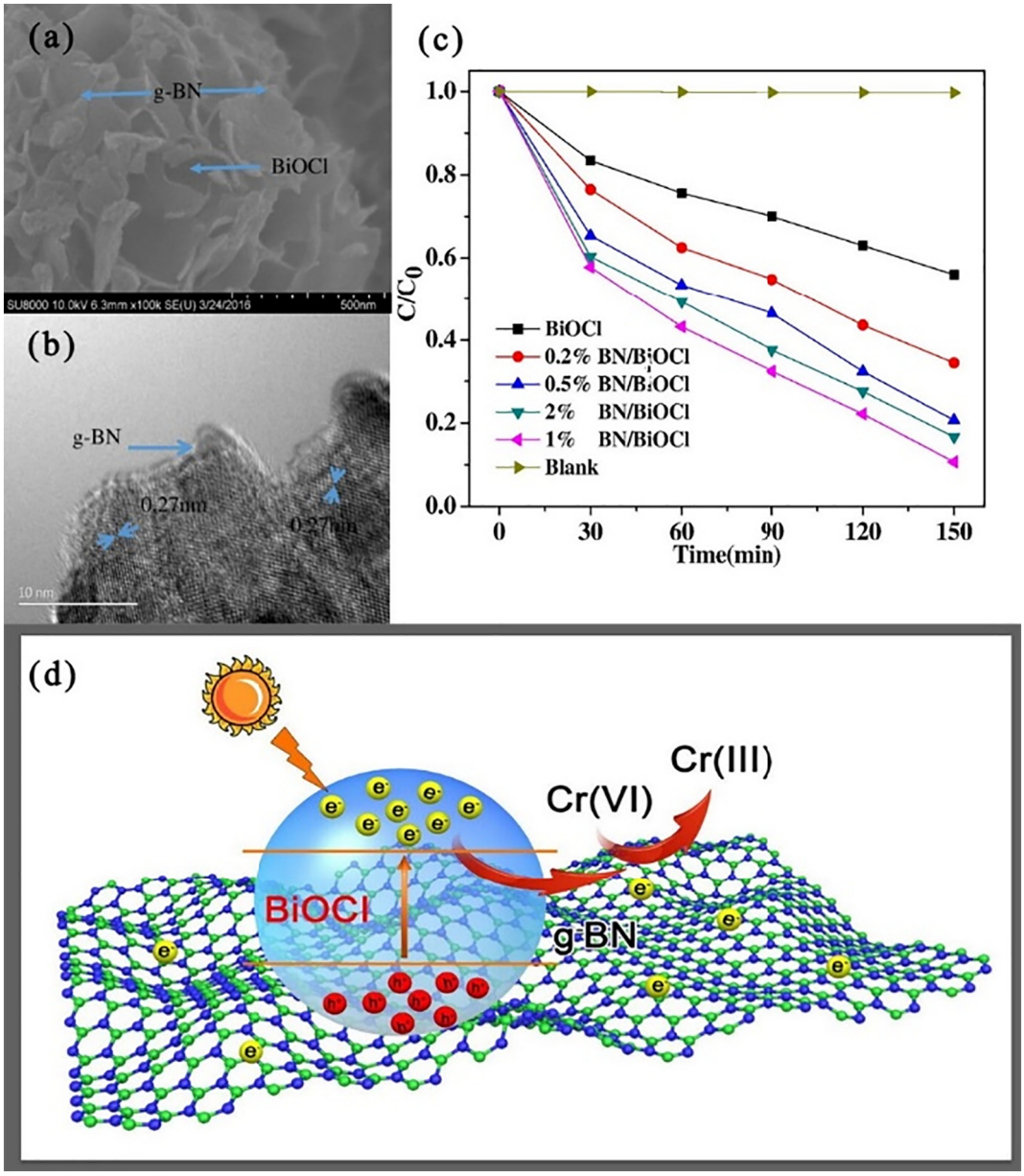

Fig. 13. (a) FESEM and (b) HRTEM of 1% BN/BiOCl composite. (b) Cr(VI) photocatalytic reduction over different photocatalysts under visible light irradiation. (c) The possible mechanism of the Cr(VI) photoreduction over the 1% BN/BiOCl composite.
(Reprinted with permission from ref. [164]. Copyright (2016) Elsevier.)

For alkaline Cr(VI) solutions:

$$Cr_2O_7^{2-} + 7H_2O + 6e^- \rightarrow 2Cr(OH)_3 + 8OH^- \quad (7)$$

Therefore, at pH 2, the as-prepared 1% BN/BiOCl nanomaterials show the best ability to photocatalytic reduction of Cr(VI) under visible light among all synthesized samples, which is about 2.39 times as high as that of bare BiOCl microspheres (Fig. 13c). This could be attributed to the doping of BN, which enhances the adsorption properties of BiOCl, improves the visible light absorption, narrows the band gap and represses the recombination of photo-generated electro-hole pairs. The possible mechanism is depicted in Fig. 13d, under visible light irradiation, the electrons of BiOCl excite from the VB to the CB leaving holes in the VB, and then the photo-generated electrons in the VB can be strapped and transferred by BN to convert adsorbed Cr(VI) to Cr(III) [164].

The adsorption ability for heavy metal ions of BiOX nanomaterials in photocatalytic reduction process cannot be ignored. Li's group [165] discovered that flower-like BiOBr nanomaterials can serve as adsorbents for removal of Cr(VI) ions in a wide pH range. Owing to their loosely structure and big specific surface area, the flower-like BiOBr nanostructures obtained from microwave irradiation method show a satisfactory removal ability for Cr(VI) ions. Based on this, their team has developed a series of BiOX nanostructures synthesized by a microwave assisted method in mannitol solution [166]. Among them, the flower-like hierarchical BiOX nanostructures exhibited much stronger Cr(VI) removal capacity than other BiOX nanostructures, which can be also ascribed to their highly specific surface areas and unique hierarchical structures. Compared with flower-like BiOCl and BiOBr nanomaterials, however, flower-like BiOI nanomaterials showed relatively weaker Cr (VI) adsorption efficiency [166]. This could be closely related to their inherent properties, such as BET surface area, distribution of surface charge, isoelectric point (IEP) and so on. The IEP of flower-like BiOCl,

BiOBr and BiOI nanomaterials was estimated about 1.9, 2.6 and 0.9, respectively. Thus, the relatively negative IEP of flower-like BiOI nanomaterials may leads to its weak removal ability for negatively Cr (VI) species ($HCrO_4^-$ and $Cr_2O_7^{2-}$) [166].

These results highlight the latent capacity of BiOX photocatalytic nanomaterials in photocatalytic removal of heavy metal ions, which is an efficient and energy efficient method for removal of hazardous heavy metal ions. In particular, with the help of some strategies, such as co-catalyst [164], crystal facet control [57,62,63], heterojunction [167,168], bismuth-rich strategy [113,115] and solid solutions [115], the removal efficiency of heavy metal ions by BiOX nanomaterials under visible light irradiation is greatly enhanced. Progress achieved in this field may push the BiOX-based photocatalytic systems for heavy metal ions removal to a higher efficient direction.

5.3. Photocatalytic oxidation of air contaminants

With the deterioration of atmospheric quality, air pollution has attracted more and more attention. A number of methods have been established to purify polluted air, such as physical adsorption, catalysis redox, biofiltration and so on [169,170]. Compared with these techniques, photocatalytic oxidation is of the highest efficiency with recyclable characteristics, and without secondary pollution. Therefore, hierarchical BiOX photocatalytic nanomaterials as a novel ternary oxide semiconductor are widely used to remove air pollutants due to their distinctive physical, chemical and optical properties, etc. Ai et al. [171] fabricated BiOBr microspheres via a nonaqueous sol-gel method for removal of NO under visible light irradiation. The as-synthesized samples showed superior photocatalytic activity to the Degussa TiO_2 P25 and C doped TiO_2 as well as BiOBr bulk powder. This is mainly due to their suitable band gap and special hierarchical structure, which could enhance their absorption efficiency of visible light and accelerate the diffusion of intermediates, respectively. The major reaction steps of this photocatalytic oxidation of NO are displayed by the following equations (Eqs. (8)–(11)) [171].

$$NO + 2{\cdot}OH \rightarrow NO_2 + H_2O \quad (8)$$

$$NO_2 + {\cdot}OH \rightarrow NO_3^- + H^+ \quad (9)$$

$$NO + NO_2 + H_2O \rightarrow 2HNO_2 \quad (10)$$

$$NO_x + {\cdot}O_2^- \rightarrow NO_3^- \quad (11)$$

Apart from microstructure modulation, other strategies such as solid solutions [105,172,173], photosensitization [174], surface metal ion

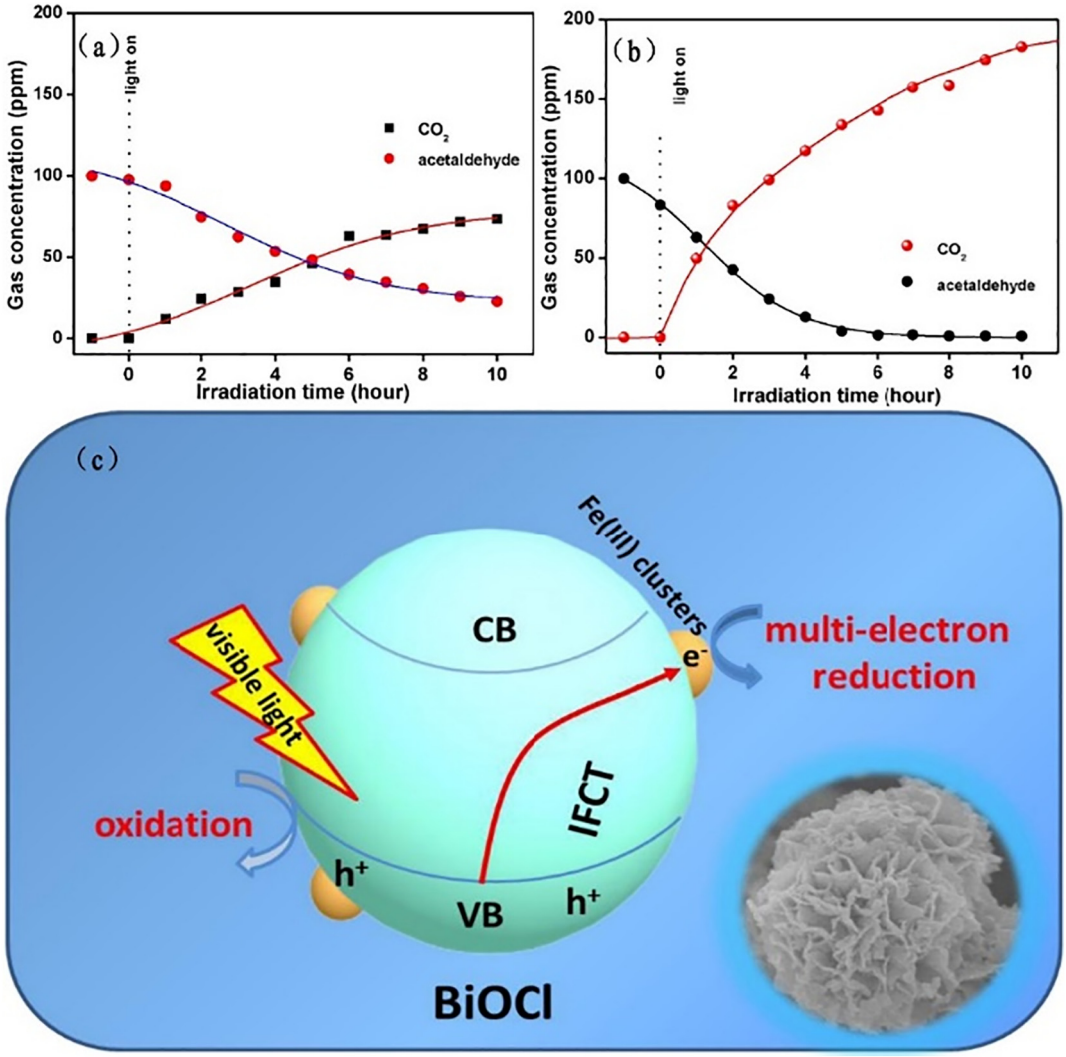

Fig. 14. Concentration of gaseous acetaldehyde on (a) BiOCl and (b) Fe(III)–BiOCl under visible light irradiation. (c) Diagram of the photo-induced electrons separation and migration in the Fe(III)–BiOCl under visible light irradiation.
(Reprinted with permission from ref. [175]. Copyright (2015) Elsevier).

clusters modification [175,176], heterojunction [177–179], facets and defects controlling [60,179] and surface plasmon resonance (SPR) [60] have been verified as efficient avenues to improve the ability of BiOX photocatalytic nanomaterials for removal of air pollutants under visible light. For example, Huang and co-workers [175] investigated the visible light photocatalytic activity of Fe(III)-BiOCl and bare BiOCl by the decomposition of gaseous acetaldehyde, and their obtained results demonstrated that the Fe(III)-BiOCl showed higher photocatalytic performance, as displayed in Fig. 14a and b. This can be attributed to the Fe(III) clusters fixed on the surfaces of BiOCl, they can promote the separation of photo-induced charge carriers through interfacial charge transfer (IFCT) under visible light illumination and serve as the centers of redox for the multi-electron reduction reaction of O_2 (Fig. 14c) [175]. The electrons in the VB of BiOCl microflowers are induced and migrated to the Fe(III) clusters by the IFCT process under visible light illumination. Subsequently the Fe(III) clusters are reduced to the Fe(II) clusters, which can act as the multi-electron redox site for the O_2 reduction and thus are oxidized to the Fe(III) clusters. Meanwhile, the generated holes in the VB of BiOCl can degrade the gaseous acetaldehyde because of their great oxidation power. Moreover, their team discovered that the Rh(III) clusters can also improve the ability of BiOCl for photocatalytic decompose gaseous acetaldehyde [176]. Their work indicates that surface transition metal ion clusters modification could greatly improve the visible light photocatalytic capacity of BiOX photocatalysts.

Very recently, Dong et al. developed Bi@BiOCl plasmonic photocatalysts with exposed facets, oxygen defects and plasmonic Bi metal for removal of NO under visible light [60]. In contrast to pure BiOCl and Ag@BiOCl, Bi@BiOCl exhibited enhanced visible light induced photocatalytic oxidation ability for NO. And the Bi@BiOCl with suitable Bi metal concentration and exposed {010} facets (B010-Bi30) displayed the highest photocatalytic activity. This distinct enhancement is due to their improved separation ability of charge carriers and favorable morphological structure [60]. This work provides a new strategy to construct efficient BiOX photocatalysts for removal of NO using facets, defects and SPR effects.

However, Dong et al. [180] utilized the BiOI hollow microspheres for removing NO under visible light and they found out that the generated NO_3^- could restrict •OH generation through occupying the surface active sites of BiOI microspheres. OH^- can't be adsorbed again and •OH can't be produced because like charges repel each other. Therefore, NO is directly oxidized to NO_2 by photo-generated holes. Thus, this greatly affects its ability for photocatalytic oxidation of NO.

To overcome this disadvantage, Xia et al. [181] designed a BiOI/Al_2O_3-padded trickling scrubber used for simultaneous removal of SO_2 and NO under visible light irradiation. The SO_2 and NO removal efficiencies in this photocatalytic trickling scrubber system can reach 100% and it could be attributed to the fact that the improved gas absorption capacity and massive reactive •OH production. The recycled activity tests indicated that this system is stable for long-term continuous elimination of SO_2 and NO [181]. This study demonstrates that the BiOI/Al_2O_3-padded trickling scrubber possess an immense application potential for simultaneous removal of SO_2 and NO. In general, some researches have been done on the treatment of air pollutants with BiOX photocatalytic nanomaterials, and the results show that the modified BiOX photocatalysts do have great potential for remove air pollutants.

6. Conclusion and perspectives

In the past few decades, many advances have been made to use BiOX photocatalytic nanomaterials for addressing energy and environmental challenges. The unique properties of BiOX have provided more possibilities to improve their visible light photocatalytic activity. In this review, we summarize the recent studies in the fields of water splitting, reduction of CO_2, removal of environmental pollutants based on BiOX photocatalytic nanomaterials. Our purposes are to review the current research on the strategies for the enhancement of BiOX-based photocatalytic activities in energy conversion and environmental management, which will give guidelines for future research. Although progresses have been made in the field of BiOX photocatalytic nanomaterials over recent years, the BiOX photocatalysts which still in experimental stage cannot satisfy the demand of practical production applications. Significant challenges remain in the construction of BiOX-based photocatalytic systems with high photocatalytic efficiency in energy conversion and environmental management.

First, since BiOX have many different crystal facets, besides the common {001} and {010} facet-dominant BiOX, the facile synthesis of BiOX photocatalysts exposed with other high-performance crystal facets are also essential. In addition, as a result of the difference between crystal facets, the free radicals produced by these crystal facets may be diverse, this requires us to further explore the reaction mechanism between different facets to find the optimal crystal facet.

Second, the IEF intensity originated from the unique layered structure is an interesting characteristic of BiOX photocatalysts, however, the study of the effect of IEF on photocatalysis of BiOX is still lacking. Further research should focus on the specific mechanism of photocatalysis under the effect of IEF and the development of strategies for enhancing photocatalytic activities of BiOX-based on the changes of IEF.

Third, in future research on the hydrogen production by photocatalytic water splitting based on BiOX nanomaterials, in addition to the in-depth investigation of the reaction mechanisms and development of efficient hydrogen production system, a study of the stability and sustainability of BiOX photocatalysts in practical application should be performed. There are some other difficulties that must be overcome to achieve high yield of hydrogen and meet practical applications, such as the simultaneous generation of H_2 and O_2, the separation of H_2 and O_2 and the design for large-scale reactors.

Fourth, the products are complex and diverse when use BiOX photocatalysts to reduce CO_2. In order to obtain single and stable fuel, it will be necessary to clarify the reaction mechanism and find the optimal reaction condition. Moreover, the effect of BiOX nanostructures on CO_2 molecules capture should also be discussed.

Fifth, the contaminants management by BiOX nanomaterials now mainly focus on dyes, Cr(VI) and NO. But for complex organic pollutants, especially toxic and refractory pollutants, other hazardous heavy ions and air contaminants, the relative reports are very deficient. Besides, the abilities of BiOX nanomaterials to tackle co-contamination are still unclear and they need further exploration.

Acknowledgments

This study was financially supported by the National Natural Science Foundation of China (51521006, 51378190, 51579098, 51408206), the Program for Changjiang Scholars and Innovative Research Team in University (IRT-13R17), the National Program for Support of Top-Notch Young Professionals of China (2014), the Program for New Century Excellent Talents in University (NCET-13-0186), Scientific Research Fund of Hunan Provincial Education Department (521293050), Hunan Provincial Science and Technology Plan Project (No. 2016RS3026) and Shanghai Tongji Gao Tingyao Environmental Science and Technology Development Foundation (2016).

References

[1] Zeng G, Chen M, Zeng Z. Science 2013;340:1403.
[2] Zeng G, Chen M, Zeng Z. Nature 2013;499:154.
[3] Cheng M, Zeng G, Huang D, Lai C, Xu P, Zhang C, et al. Chem Eng J 2016;284:582.
[4] Cheng M, Zeng G, Huang D, Yang C, Lai C, Zhang C, et al. Chem Eng J 2017;314:98.
[5] Zou Z, Ye J, Sayama K, Arakawa H. Nature 2001;414:625.
[6] Kudo A, Miseki Y. Chem Soc Rev 2009;38:253.
[7] Inoue T, Fujishima A, Konishi S, Honda K. Nature 1979;277:637.
[8] Habisreutinger SN, Schmidt-Mende L, Stolarczyk JK. Angew Chem Int Ed Engl 2013;52:7372.

[9] Chatterjee D, Dasgupta S. J Photochem Photobiol C Photchem Rev 2005;6:186.
[10] Gaya UI, Abdullah AH. J Photochem Photobiol C Photchem Rev 2008;9:1.
[11] Hoffmann MR, Martin ST, Choi W, Bahnemann DW. Chem Rev 1995;95:69.
[12] Fujishima A. Nature 1972;238:37.
[13] Fox MA, Dulay MT. Chem Rev 1993;93:341.
[14] Chen F, Yang Q, Wang Y, Zhao J, Wang D, Li X, et al. Appl Catal Environ 2017;205:133.
[15] Wang H, Yuan X, Wu Y, Zeng G, Dong H, Chen X, et al. Appl Catal Environ 2016;186:19.
[16] Xiang Q, Yu J, Jaroniec M. Chem Soc Rev 2012;41:782.
[17] Lai C, Wang M-M, Zeng G-M, Liu Y-G, Huang D-L, Zhang C, et al. Appl Surf Sci 2016;390:368.
[18] Linsebigler AL, Lu G. Yates Jr JT. Chem Rev 1995;95:735.
[19] Pelaez M, Nolan NT, Pillai SC, Seery MK, Falaras P, Kontos AG, et al. Appl Catal Environ 2012;125:331.
[20] Chen C, Ma W, Zhao J. Chem Soc Rev 2010;39:4206.
[21] Hosogi Y, Shimodaira Y, Kato H, Kobayashi H, Kudo A. Chem Mater 2008;20:1299.
[22] Cao S, Zhou P, Yu J. Chin J Catal 2014;35:989.
[23] Meng X, Zhang Z. J Mol Catal A Chem 2016;423:533.
[24] Wang J, Tang L, Zeng G, Deng Y, Liu Y, Wang L, et al. Appl Catal Environ 2017;209:285.
[25] Wang H, Yuan X, Wu Y, Zeng G, Tu W, Sheng C, et al. Appl Catal Environ 2017;209:543.
[26] Chen F, Yang Q, Li X, Zeng G, Wang D, Niu C, et al. Appl Catal Environ 2017;200:330.
[27] Zhao L, Zhang X, Fan C, Liang Z, Han P. Phys B: Condens Matter 2012;407:3364.
[28] Zhang K, Liu C, Huang F, Zheng C, Wang W. Appl Catal Environ 2006;68:125.
[29] Huang WL, Zhu Q. Comput Mater Sci 2008;43:1101.
[30] Ye L, Su Y, Jin X, Xie H, Zhang C. Environ Sci Nano 2014;1:90.
[31] Zhou C, Lai C, Xu P, Zeng G, Huang D, Zhang C, et al. ACS Sustain Chem Eng 2018;6:4174.
[32] Li J, Yu Y, Zhang L. Nanoscale 2014;6:8473.
[33] Cheng H, Huang B, Dai Y. Nanoscale 2014;6:2009.
[34] Zhang X, Ai Z, Jia F, Zhang L. J Phys Chem C 2008;112:747.
[35] Stampfl C, Van de Walle C. Phys Rev B 1999;59:5521.
[36] Jin J, Wang Y, He T. RSC Adv 2015;5:100244.
[37] Zhang J, Shi F, Lin J, Chen D, Gao J, Huang Z, et al. Chem Mater 2008;20:2937.
[38] Wu D, Ye L, Yip HY, Wong PK. Cat Sci Technol 2017;7:265.
[39] An H, Du Y, Wang T, Wang C, Hao W, Zhang J. Rare Metals 2008;27:243.
[40] Long Y, Wang Y, Zhang D, Ju P, Sun Y. J Colloid Interface Sci 2016;481:47.
[41] Xu P, Zeng GM, Huang DL, Feng CL, Hu S, Zhao MH, et al. Sci Total Environ 2012;424:1.
[42] Huang D, Wang Y, Zhang C, Zeng G, Lai C, Wan J, et al. RSC Adv 2016;6:73186.
[43] Wang C, Shao C, Liu Y, Zhang L. Scr Mater 2008;59:332.
[44] Jiang J, Zhao K, Xiao X, Zhang L. J Am Chem Soc 2012;134:4473.
[45] Gao M, Zhang D, Pu X, Li H, Li J, Shao X, et al. Mater Lett 2015;140:31.
[46] Zhang D, Li J, Wang Q, Wu Q. J Mater Chem A 2013;1:8622.
[47] Ye L, Zan L, Tian L, Peng T, Zhang J. Chem Commun 2011;47:6951.
[48] Zhang G, Su A, Qu J, Xu Y. Mater Res Bull 2014;55:43.
[49] Zhao Y, Tan X, Yu T, Wang S. Mater Lett 2016;164:243.
[50] Huo Y, Zhang J, Miao M, Jin Y. Appl Catal Environ 2012;111–112:334.
[51] Xia J, Yin S, Li H, Xu H, Yan Y, Zhang Q. Langmuir 2011;27:1200.
[52] Yang HG, Sun CH, Qiao SZ, Zou J, Liu G, Smith SC, et al. Nature 2008;453:638.
[53] Jiang Z-Y, Kuang Q, Xie Z-X, Zheng L-S. Adv Funct Mater 2010;20:3634.
[54] Ye L, Jin X, Ji X, Liu C, Su Y, Xie H, et al. Chem Eng J 2016;291:39.
[55] Pan M, Zhang H, Gao G, Liu L, Chen W. Environ Sci Technol 2015;49:6240.
[56] Ong WJ, Tan LL, Chai SP, Yong ST, Mohamed AR. ChemSusChem 2014;7:690.
[57] Li H, Zhang L. Nanoscale 2014;6:7805.
[58] Li Q, Zhao X, Yang J, Jia CJ, Jin Z, Fan W. Nanoscale 2015;7:18971.
[59] Li J, Zhao K, Yu Y, Zhang L. Adv Funct Mater 2015;25:2189.
[60] Dong F, Xiong T, Yan S, Wang H, Sun Y, Zhang Y, et al. J Catal 2016;344:401.
[61] Zhang H, Yang Y, Zhou Z, Zhao Y, Liu L. J Phys Chem C 2014;118:14662.
[62] Fan Z, Zhao Y, Zhai W, Qiu L, Li H, Hoffmann MR. RSC Adv 2016;6:2028.
[63] Han J, Zhu G, Hojamberdiev M, Peng J, Zhang X, Liu Y, et al. New J Chem 2015;39:1874.
[64] Chen X, Liu L, Peter YY, Mao SS. Science 2011;331:746.
[65] Ye L, Deng K, Xu F, Tian L, Peng T, Zan L. Phys Chem Chem Phys 2012;14:82.
[66] Ihara T. Appl Catal Environ 2003;42:403.
[67] Nowotny M, Sheppard L, Bak T, Nowotny J. J Phys Chem C 2008;112:5275.
[68] Zhang L, Wang W, Jiang D, Gao E, Sun S. Nano Res 2014;8:821.
[69] Wang XJ, Zhao Y, Li FT, Dou LJ, Li YP, Zhao J, et al. Sci Rep 2016;6:24918.
[70] Guan M, Xiao C, Zhang J, Fan S, An R, Cheng Q, et al. J Am Chem Soc 2013;135:10411.
[71] Chen M, Yu S, Zhang X, Wang F, Lin Y, Zhou Y. Superlattice Microstruct 2016;89:275.
[72] Katsnelson MI. Mater Today 2007;10:20.
[73] Wang H, Yuan X, Wu Y, Huang H, Peng X, Zeng G, et al. Adv Colloid Interface Sci 2013;195–196:19.
[74] Wang H, Yuan X, Zeng G, Wu Y, Liu Y, Jiang Q, et al. Adv Colloid Interface Sci 2015;221:41.
[75] Dong S, Pi Y, Li Q, Hu L, Li Y, Han X, et al. J Alloys Compd 2016;663:1.
[76] Jiang T, Li J, Sun Z, Liu X, Lu T, Pan L. Ceram Int 2016;42:16463.
[77] Liu Z, Xu W, Fang J, Xu X, Wu S, Zhu X, et al. Appl Surf Sci 2012;259:441.
[78] Yan Y, Miao J, Yang Z, Xiao F-X, Yang HB, Liu B, et al. Chem Soc Rev 2015;44:3295.
[79] Vadivel S, Theerthagiri J, Madhavan J, Santhoshini Priya T, Balasubramanian N. J Water Proc Eng 2016;10:165.
[80] Xia J, Di J, Yin S, Li H, Xu L, Xu Y, et al. Ceram Int 2014;40:4607.
[81] Weng B, Xu F, Xu J. J Nanopart Res 2014;16:2766.
[82] Li H, He X, Kang Z, Huang H, Liu Y, Liu J, et al. Angew Chem Int Ed Engl 2010;49:4430.
[83] Di J, Xia J, Ji M, Wang B, Yin S, Zhang Q, et al. ACS Appl Mater Interfaces 2015;7:20111.
[84] Xia J, Di J, Li H, Xu H, Li H, Guo S. Appl Catal Environ 2016;181:260.
[85] Long B, Huang Y, Li H, Zhao F, Rui Z, Liu Z, et al. Ind Eng Chem Res 2015;54:12788.
[86] Di J, Xia J, Ji M, Xu L, Yin S, Zhang Q, et al. Carbon 2016;98:613.
[87] Zhang C, Lai C, Zeng G, Huang D, Yang C, Wang Y, et al. Water Res 2016;95:103.
[88] Huang D, Liu L, Zeng G, Xu P, Huang C, Deng L, et al. Chemosphere 2017;174:545.
[89] Li M, Huang H, Yu S, Tian N, Dong F, Du X, et al. Appl Surf Sci 2016;386:285.
[90] Wang H, Zhang L, Chen Z, Hu J, Li S, Wang Z, et al. Chem Soc Rev 2014;43:5234.
[91] Yu L, Zhang X, Li G, Cao Y, Shao Y, Li D. Appl Catal Environ 2016;187:301.
[92] Kandi D, Martha S, Thirumurugan A, Parida KM. J Phys Chem C 2017;121:4834.
[93] Di J, Xia J, Ge Y, Xu L, Xu H, Chen J, et al. Dalton Trans 2014;43:15429.
[94] Xiang Y, Ju P, Wang Y, Sun Y, Zhang D, Yu J. Chem Eng J 2016;288:264.
[95] Kong L, Jiang Z, Xiao T, Lu L, Jones MO, Edwards PP. Chem Commun (Camb) 2011;47:5512.
[96] Mao W, Bao K, Cao F, Chen B, Liu G, Wang W, et al. Ceram Int 2017;43:3363.
[97] Li W, Tian Y, Li H, Zhao C, Zhang B, Zhang H, et al. Appl Catal Gen 2016;516:81.
[98] Gao S, Guo C, Lv J, Wang Q, Zhang Y, Hou S, et al. Chem Eng J 2017;307:1055.
[99] Luo J, Zhou X, Ma L, Xu X. J Mol Catal A Chem 2015;410:168.
[100] Chang X, Yu G, Huang J, Li Z, Zhu S, Yu P, et al. Catal Today 2010;153:193.
[101] Maeda K, Teramura K, Lu D, Takata T, Saito N, Inoue Y, et al. Nature 2006;440:295.
[102] Zhang J, Han Q, Zhu J, Wang X. J Colloid Interface Sci 2016;477:25.
[103] Yang Z, Cheng F, Dong X, Cui F. RSC Adv 2015;5:68151.
[104] Zhang Y, Sun X, Yang G, Zhu Y, Si H, Zhang J, et al. Mater Sci Semicond Process 2016;41:193.
[105] Ou M, Dong F, Zhang W, Wu Z. Chem Eng J 2014;255:650.
[106] Asahi R, Morikawa T, Ohwaki T, Aoki K, Taga Y. Science 2001;293:269.
[107] Wang P-Q, Liu J-Y, Hu Y-Q, Bai Y, Fan Z. Micro Nano Lett 2012;7:876.
[108] Jiang G, Li X, Wei Z, Jiang T, Du X, Chen W. Powder Technol 2014;260:84.
[109] Zhang S, Wang D, Song L. Mater Chem Phys 2016;173:298.
[110] Gao M, Zhang D, Pu X, Li H, Li W, Shao X, et al. Sep Purif Technol 2016;162:114.
[111] Li WT, Huang WZ, Zhou H, Yin HY, Zheng YF, Song XC. J Alloys Compd 2015;638:148.
[112] Han X, Dong S, Yu C, Wang Y, Yang K, Sun J. J Alloys Compd 2016;685:997.
[113] Shang J, Hao W, Lv X, Wang T, Wang X, Du Y, et al. ACS Catal 2014;4:954.
[114] Ye L, Jin X, Liu C, Ding C, Xie H, Chu KH, et al. Appl Catal Environ 2016;187:281.
[115] Bai Y, Ye L, Chen T, Wang P, Wang L, Shi X, et al. Appl Catal Environ 2017;203:633.
[116] Zhang L, Wang W, Sun S, Sun Y, Gao E, Xu J. Appl Catal Environ 2013;132–133:315.
[117] Zhang L, Wang W, Sun S, Jiang D, Gao E. Appl Catal Environ 2015;162:470.
[118] Ye L, Jin X, Leng Y, Su Y, Xie H, Liu C. J Power Sources 2015;293:409.
[119] Li J, Li H, Zhan G, Zhang L. Acc Chem Res 2017;50:112.
[120] Si HY, Mao CJ, Xie YM, Sun XG, Zhao JJ, Zhou N, et al. Dalton Trans 2016;46:200.
[121] Wu D, Ye L, Yue S, Wang B, Wang W, Yip HY, et al. J Phys Chem C 2016;120:7715.
[122] Kong XY, Lee WPC, Ong W-J, Chai S-P, Mohamed AR. ChemCatChem 2016;8:3074.
[123] Bai Y, Ye L, Wang L, Shi X, Wang P, Bai W. Environ Sci Nano 2016;3:902.
[124] Ye L, Wang H, Jin X, Su Y, Wang D, Xie H, et al. Solar Energy Mater Solar Cells 2016;144:732.
[125] Wang JC, Yao HC, Fan ZY, Zhang L, Wang JS, Zang SQ, et al. ACS Appl Mater Interfaces 2016;8:3765.
[126] Tang ZK, Yin WJ, Le Z, Wen B, Zhang DY, Liu LM, et al. Sci Rep 2016;6:32764.
[127] Zhang L, Han Z, Wang W, Li X, Su Y, Jiang D, et al. Chemistry 2015;21:18089.
[128] Dai W-W, Zhao Z-Y, Ballato J. J Am Ceram Soc 2016;99:3015.
[129] Zhang X, Li B, Wang J, Yuan Y, Zhang Q, Gao Z, et al. Phys Chem Chem Phys 2014;16:25854.
[130] Zhao Z-Y, Dai W-W. Inorg Chem 2015;54:10732.
[131] Li J, Zhan G, Yu Y, Zhang L. Nat Commun 2016;7:11480.
[132] Izumi Y. Coord Chem Rev 2013;257:171.
[133] Sakakura T, Choi J-C, Yasuda H. Chem Rev 2007;107:2365.
[134] Roy SC, Varghese OK, Paulose M, Grimes CA. ACS Nano 2010;4:1259.
[135] Song G, Wu X, Xin F, Yin X. Front Chem Sci Eng 2017;11:197.
[136] Huang DL, Zeng GM, Feng CL, Hu S, Jiang XY, Tang L, et al. Environ Sci Technol 2008;42:4946.
[137] Zhang Y, Zeng GM, Tang L, Huang DL, Jiang XY, Chen YN. Biosens Bioelectron 2007;22:2121.
[138] Tang L, Zeng GM, Shen GL, Li YP, Zhang Y, Huang DL. Environ Sci Technol 2008;42:1207.
[139] Cheng Y, He H, Yang C, Zeng G, Li X, Chen H, et al. Biotechnol Adv 2016;34:1091.
[140] Yang C, Chen H, Zeng G, Yu G, Luo S. Biotechnol Adv 2010;28:531.
[141] Huang D, Hu C, Zeng G, Cheng M, Xu P, Gong X, et al. Sci Total Environ 2017;574:1599.
[142] Deng Y, Tang L, Zeng G, Zhu Z, Yan M, Zhou Y, et al. Appl Catal Environ 2017;203:343.
[143] Gong JL, Wang B, Zeng GM, Yang CP, Niu CG, Niu QY, et al. J Hazard Mater 2009;164:1517.
[144] Zhou C, Lai C, Huang D, Zeng G, Zhang C, Cheng M, et al. Appl Catal Environ 2018;220:202.
[145] Hao R, Xiao X, Zuo X, Nan J, Zhang W. J Hazard Mater 2012;209–210:137.
[146] Di J, Xia J, Ji M, Wang B, Yin S, Zhang Q, et al. Appl Catal Environ 2016;183:254.
[147] Yu Y, Cao C, Liu H, Li P, Wei F, Jiang Y, et al. J Mater Chem A 2014;2:1677.
[148] Jia X, Cao J, Lin H, Zhang M, Guo X, Chen S. Appl Catal Environ 2017;204:505.
[149] Cheng H, Huang B, Wang P, Wang Z, Lou Z, Wang J, et al. Chem Commun (Camb) 2011;47:7054.
[150] Chen F, Yang Q, Sun J, Yao F, Wang S, Wang Y, et al. ACS Appl Mater Interfaces 2016;8:32887.

[151] Xiao X, Tu S, Lu M, Zhong H, Zheng C, Zuo X, et al. Appl Catal Environ 2016;198:124.
[152] Fu H, Pan C, Yao W, Zhu Y. J Phys Chem B 2005;109:22432.
[153] Xiao Y, Song X, Liu Z, Li R, Zhao X, Huang Y. J Ind Eng Chem 2017;45:248.
[154] Li J, Sun S, Qian C, He L, Chen KK, Zhang T, et al. Chem Eng J 2016;297:139.
[155] Xu F, Cheng G, Song S, Wei Y, Chen R. ACS Sustain Chem Eng 2016;4:7013.
[156] Zhang C, Lai C, Zeng G, Huang D, Tang L, Yang C, et al. Biosens Bioelectron 2016;81:61.
[157] Zeng G, Zhang C, Huang D, Lai C, Tang L, Zhou Y, et al. Biosens Bioelectron 2017;90:542.
[158] Feng Y, Gong J-L, Zeng G-M, Niu Q-Y, Zhang H-Y, Niu C-G, et al. Chem Eng J 2010;162:487.
[159] Fan T, Liu Y, Feng B, Zeng G, Yang C, Zhou M, et al. J Hazard Mater 2008;160:655.
[160] Hu XJ, Wang JS, Liu YG, Li X, Zeng GM, Bao ZL, et al. J Hazard Mater 2011;185:306.
[161] Zhang C, Zeng G, Huang D, Lai C, Huang C, Li N, et al. RSC Adv 2014;4:55511.
[162] Huang D, Xue W, Zeng G, Wan J, Chen G, Huang C, et al. Water Res 2016;106:15.
[163] Qamar M, Yamani ZH. Appl Catal Gen 2012;439–440:187.
[164] Xu H, Wu Z, Ding M, Gao X. Mater Des 2017;114:129.
[165] Li G, Qin F, Yang H, Lu Z, Sun H, Chen R. Eur J Inorg Chem 2012;2012:2508.
[166] Li G, Qin F, Wang R, Xiao S, Sun H, Chen R. J Colloid Interface Sci 2013;409:43.
[167] Wang Q, Shi X, Liu E, Crittenden JC, Ma X, Zhang Y, et al. J Hazard Mater 2016;317:8.
[168] Wang K, Shao C, Li X, Zhang X, Lu N, Miao F, et al. Cat Com 2015;67:6.
[169] Ahmaruzzaman M. Prog Energy Combust Sci 2010;36:327.
[170] Zhao L, Li C, Li S, Wang Y, Zhang J, Wang T, et al. Appl Catal Environ 2016;198:420.
[171] Ai Z, Ho W, Lee S, Zhang L. Environ Sci Technol 2009;43:4143.
[172] Dong F, Sun Y, Fu M, Wu Z, Lee SC. J Hazard Mater 2012;219–220:26.
[173] Wu T, Li X, Zhang D, Dong F, Chen S. J Alloys Compd 2016;671:318.
[174] Li G, Jiang B, Xiao S, Lian Z, Zhang D, Yu JC, et al. Environ Sci: Processes Impacts 2014;16:1975.
[175] Huang C, Hu J, Cong S, Zhao Z, Qiu X. Appl Catal Environ 2015;174–175:105.
[176] Hu J, Wu X, Huang C, Fan W, Qiu X. Appl Surf Sci 2016;387:45.
[177] Ai Z, Ho W, Lee S. J Phys Chem C 2011;115:25330.
[178] Sun Y, Zhang W, Xiong T, Zhao Z, Dong F, Wang R, et al. J Colloid Interface Sci 2014;418:317.
[179] Zhou R, Wu J, Zhang J, Tian H, Liang P, Zeng T, et al. Appl Catal Environ 2017;204:465.
[180] Dong G, Ho W, Zhang L. Appl Catal Environ 2015;168–169:490.
[181] Xia D, Hu L, He C, Pan W, Yang T, Yang Y, et al. Chem Eng J 2015;279:929.